J. Math. Biol.
DOI 10.1007/s00285-011-0484-7

Mathematical Biology

Generalized spin models for coupled cortical feature maps obtained by coarse graining correlation based synaptic learning rules

Peter J. Thomas · Jack D. Cowan

Received: 13 August 2010 / Revised: 11 June 2011

Abstract We derive generalized spin models for the development of feedforward cortical architecture from a Hebbian synaptic learning rule in a two layer neural network with nonlinear weight constraints. Our model takes into account the effects of lateral interactions in visual cortex combining local excitation and long range effective inhibition. Our approach allows the principled derivation of developmental rules for low-dimensional feature maps, starting from high-dimensional synaptic learning rules. We incorporate the effects of smooth nonlinear constraints on net synaptic weight projected from units in the thalamic layer (the fan-out) and on the net synaptic weight received by units in the cortical layer (the fan-in). These constraints naturally couple together multiple feature maps such as orientation preference and retinotopic organization. We give a detailed illustration of the method applied to the development of the orientation preference map as a special case, in addition to deriving a model for joint pattern formation in cortical maps of orientation preference, retinotopic location, and receptive field width. We show that the combination of Hebbian learning and center-surround cortical interaction naturally leads to an orientation map development model that is closely related to the XY magnetic lattice model from statistical physics. The results presented here provide justification for phenomenological models studied in Cowan and Friedman (Advances in neural information processing systems 3, 1991), Thomas and Cowan (Phys Rev Lett 92(18):e188101, 2004) and provide a

P. J. Thomas (✉)
Department of Mathematics, Case Western Reserve University, Cleveland, OH, USA
e-mail: pjthomas@case.edu

J. D. Cowan
Department of Mathematics, The University of Chicago, Chicago, IL, USA

Published online: 19 November 2011

developmental model realizing the synaptic weight constraints previously assumed in Thomas and Cowan (Math Med Biol 23(2):119–138, 2006).

Keywords Coarse graining · Visual cortex · Hebbian learning · XY model · Orientation map · Mexican hat · Nonlinear eigenvalue problem · Pattern formation · Symmetry breaking

Mathematics Subject Classification (2000) 92C15 · 92C20 · 37N25

1 Introduction

Orientation tuning, the selective response of cortical neurons to the angle of visual stimuli such as bars, gratings or edges, is a particularly well studied feature of cortical physiology (Hubel and Wiesel 1974; Wiesel and Hubel 1974). In many species orientation selectivity is absent in the response of retinal ganglion cells and individual cells in the visual thalamus, and first appears in the input layers of primary visual cortex. In the visual cortex of primates and cats, inter alia,[1] orientation preferences are organized into a *topographic map*: nearby cells tend to encode similar orientations, leading to localized patches of similar orientation preference. Preferences for other visual input features, for example ocular dominance (Tootell et al. 1988), retinotopy (Tootell et al. 1988) and spatial frequency preference (Shoham et al. 1997), also exhibit spatial organization. Using voltage sensitive dyes (Blasdel and Salama 1986) and optical imaging of intrinsic signals (Malach et al. 1993) it has been shown that the spatial organization mainly comprises *linear zones*, or regions in which the orientation preference changes smoothly, and *pinwheels*, small regions in which level curves of the orientation preference map appear to converge to a point. The orientation map is approximately periodic in the following sense. Patches of cortex containing cells of the same orientation preference occur repeatedly on a typical length scale; other local repeating feature preferences, such as ocular dominance and spatial frequency, also occur in approximately periodic patches. A typical surface region containing cells representing a complete set of orientations, ocular dominance, spatial frequency, et cetera, is referred to as a hypercolumn. The map shows a combination of order on shorter length scales (up to *c.* 300 μm, the size of a hypercolumn) and disorder at longer scales. In addition to feature selectivity, the responses of cortical cells are spatially specific, responding only to stimuli in a local region of the visual field termed a *receptive field* (Hubel and Wiesel 1962).

Orientation selectivity and its spatial organization in mammalian cortex have attracted sustained interest in the neural modeling community (Erwin et al. 1995; Goodhill 2007; McLaughlin et al. 2003; Ringach 2004; Swindale 1996). At a high level of description, phenomenological models of cortical map formation have described fundamental principles that can account for map structure, for example wiring length

[1] Tree shrews, and ferrets and galagos show topographic orientation maps in cortical area V1, while rodents do not (Kaschube et al. 2010).

minimization (Chklovskii et al. 2002; Koulakov and Chklovskii 2001), competition between map smoothness (Goodhill and Cimponeriu 2000) and feature coverage (Swindale 1991; Swindale et al. 2000), self-organizing feature maps (Erwin et al. 1992a,b), magnetic lattice models (Cowan and Friedman 1991) and Potts models (Tanaka 1990), elastic net models (Giacomantonio et al. 2010; Goodhill et al. 1997), generalized deformable models (Yuille et al. 1996), and developmental pinwheel annihilation models (Wolf and Geisel 1998). Wolf and colleagues framed orientation map formation as a dynamical optimization problem involving an abstract, phenomenological order parameter, and compared the statistical distribution of pinwheels across large numbers of model planforms satisfying imposed symmetry (Wolf 2005). The pinwheel density, relative to the typical periodicity spacing, was found to match empirical data from widely separated mammalian species (Kaschube et al. 2010). A theme common to many of these models is the combination of short range recurrent excitation and medium range lateral inhibition to create periodic patterns with a characteristic length scale, through the pattern formation mechanism originally described for biological systems by Alan Turing (1952) [although alternative mechanisms continue to be proposed Ringach (2007); Paik and Ringach (2010); Wolf and Geisel (1998)]. Recent experimental and modeling work supports the existence of such *effective* center-surround filtering mechanisms (Reyes 2010) even though the longest range connections are known to be excitatory (Mooser et al. 2004).

At a finer level of description, a series of increasingly detailed models have addressed mechanisms underlying orientation tuning at the single cell and local network level (Ringach 2004). Such models typically account for the functional properties of visual cortex neurons in terms of the anatomical structure of their inputs. Hubel and Wiesel proposed a conceptual model of thalamocortical circuitry in which the geometric structure of feedforward synaptic inputs determined the orientation preferences of cortical cells (Hubel and Wiesel 1962). Major features of this conceptual framework have been validated experimentally, including the observation of elongated subfields of synaptic input in the thalamus, with the direction of elongation corresponding to the preferred orientation (Reid and Alonso 1995; Ringach 2004). In addition to the geometry of feedforward synaptic projections, there is evidence that lateral cortico-cortical connections may also play a role in determining orientation preference (Blumenfeld et al. 2006) whether via orientation-specific lateral inhibition (Ben-Yishai et al. 1995), excitation (Bartsch and van Hemmen 2001; Somers et al. 1995), or long range oriented inputs (Mooser et al. 2004).

A third class of models, including the model defined in Sect. 3, bridges the fine grained synaptic and coarse grained phenomenological models. Starting from a description of the feedforward architecture from an abstract "retina" to a "tectum", Willshaw and von der Malsburg (von der Malsburg and Willshaw 1977; Willshaw and von der Malsburg 1979), and later Häußler and von der Malsburg (1983) employed nonlinear stability analysis to study the formation of the retinotopic map in a one dimensional correlation based model. Ken Miller and colleagues studied the development of orientation and ocular dominance maps in computational models in which cortical cells had receptive fields derived from explicit synaptic weight distributions

modified by constrained correlation based learning rules (Miller 1994; Wimbauer et al. 1997a,b).

Here we describe a mathematical method for linking together the synaptic and phenomenological levels of description. Our approach studies analytically the influence of constrained correlation-based or Hebbian developmental rules acting on the feedforward synaptic weight distribution. We employ a coarse graining approach in which the detailed synaptic weight distribution is reduced to its moments: the net synaptic input to a given cortical location; the center of mass, which represents the retinotopic tuning of the cell; and the second moments, which represent the elongation (orientation tuning and strength of orientation preference) and the receptive field width. Assuming an isotropic center-surround or "Mexican hat" lateral connectivity in the cortex (Reggia and Montgomery 1996), we show that the development of the synaptic weight distribution corresponds directly to a phenomenological cortical map model of the magnetic lattice type. In particular, the developmental rule for orientation preference corresponds to the so-called XY model of statistical physics, defined in Sect. 2.

Two considerations make the XY model particularly interesting for modeling orientation preference maps. Optical imaging data (Blasdel and Salama 1986; Bonhoeffer and Grinvald 1991; Husson et al. 2007) gives spatiotemporal average preference information about local populations of cells. Microelectrode recordings give detailed information on the behavior of individual cells but usually cannot determine the spatial organization of the behavior of large numbers of cells simultaneously across and within hypercolumns. As Maldonado and Gray wrote "the variance of receptive-field properties within local clusters of cells is largely unknown" (Maldonado and Gray 1996). Monte Carlo simulations of the XY model naturally incorporate a variable degree of disorder in local receptive field properties in the form of the thermodynamic temperature (Binder and Heermann 1997). The abstract XY model can readily be generalized to incorporate experimentally observed correlations between different cortical feature maps, for instance the orientation preference and ocular dominance maps (Cho and Kim 2004, 2005).[2]

Receptive field structure varies significantly with cortical layer (Martinez et al. 2005). The thalamocortical input layer however is dominated by simple cells, the responses of which approximately represent a convolution of the input activity (in the thalamus) with different afferent On-center and Off-center weight distributions (Hawken and Parker 1987; Hirsch and Martinez 2006). In general the detailed circuitry underlying receptive field structure, orientation and other feature preferences is complicated and highly specific, and remains only partially determined experimentally (Ohki et al. 2006; Ohki and Reid 2007). Despite uncertainties about the detailed anatomy of the thalamocortical and cortico-cortical circuitry—or perhaps because of this uncertainty—simplified mathematical models play a role in developing intuition about its development. In order to keep our approach as transparent as possible we will make a number of biological simplifications. For instance, Ohshiro and Weliky showed that the correlation of activity in the lateral geniculate nucleus (visual thalamus)

[2] Cho and Kim (2004, 2005) proposed a framework similar to that examined here, but did not discuss its explicit derivation from an underlying synaptic weight model.

drops off monotonically with a nearly circularly symmetric correlation function (Ohshiro and Weliky 2006). We will focus here on the shape of the aggregate feedforward weight profile, neglecting the separate contributions of On-center and Off-center distributions. The presentation is intended as a simple case study of a technique that may be applicable to fine grained models that relax some of these assumptions. Throughout the sequel we will assume that:

1. Cortical cells in the layer of interest receive excitatory feedforward thalamocortical input that drops off monotonically with distance (in the thalamic layer) from a central peak (see Fig. 2);
2. The geometry of the feedforward thalamocortical input determines orientation preference;
3. Feedforward synaptic weights develop gradually according to a correlation based plasticity rule with soft (logistic) nonlinear fan-in and fan-out weight constraints;
4. Activity levels in the cortex are determined, on average, by feedforward thalamic input convolved with a center-surround type spatial filter representing the effects of recurrent cortico-cortical excitation and lateral inhibition.

In (1991) Cowan and Friedman introduced a spin alignment Hamiltonian as a basis for phenomenological models of cortical ocular dominance and orientation pattern formation. In (2004) Thomas and Cowan extended this class of phenomenological model to multiple components undergoing simultaneous symmetry breaking, and argued on symmetry grounds for the existence of particular multicomponent patterns, several of which bore quantitative and qualitative resemblance to patterns observed experimentally. The present paper strengthens the mathematical basis for relating synaptic and phenomenological models by formulating the relationship in terms of linearization of an explicit developmental synaptic model around a homogeneous steady state, and showing that the planar moments of the resulting synaptic weight patterns are equivalent to the coupled phenomenological multicomponent models studied in Thomas and Cowan (2004).

In Thomas and Cowan (2006) we studied the interplay of various "uniform coverage" constraints in a simple geometric model in which receptive fields were represented by elongated planar Gaussian weight profiles. We showed that the simultaneous constraints of (i) presynaptic weight normalization, (ii) uniform retinotopic mapping and (iii) postsynaptic weight normalization could only be simultaneously satisfied for a system of unoriented or circularly symmetric feedforward receptive fields. We proposed that the introduction of a nonuniform retinotopic map would allow constraints (i) and (iii) to be preserved, which led to specific predictions about the distribution of local distortion in the retinotopic map near right and left handed orientation singularities. Moreover Thomas and Cowan (2006) showed, perhaps surprisingly, that the geometric structure of right and left handed "pinwheels" are not mirror images of each other at the synaptic level, another prediction that is testable in principle. That paper did not address a dynamical model for weight development, but rather assumed (i)–(iii) as a priori constraints.

The present paper goes substantially beyond previous publications Thomas and Cowan (2004, 2006). While the analysis here is based on a planar, approximately Gaussian model for the feedforward synaptic weights, similar to that in

Thomas and Cowan (2006), it introduces a dynamical developmental model that incorporates Hebbian correlation based weight dynamics alongside soft (logistic) versions of constraints (i) and (iii), in the spirit of Häussler and von der Malsburg (1983). We note that Häussler and von der Malsburg (1983) considered only a one dimensional retina connected to a one dimensional tectum, while the model proposed here represents both the input and the output layer as planar domains. The present paper derives the type of phenomenological model which was assumed as the starting point in Thomas and Cowan (2004) from the underlying synaptic dynamics, through a pattern formation argument.

In Sect. 2 we review a class of magnetic lattice models to which our synaptic model for orientation preference ultimately reduces. Section 3 defines the geometry of the synaptic model, the coarse grained representation of synaptic feedforward architecture, and the Hebbian developmental model. Section 4 illustrates the derivation of dynamical equations for the coarse grained variables from the Hebbian dynamics governing the synaptic weights. As a special case of the general method we show how the Hebbian learning rule combined with center-surround cortical interaction leads to the XY magnetic lattice model for orientation map development in Sect. 4.3. We conclude with a brief discussion in Sect. 5.

2 Magnetic lattice models for cortical feature maps

Cowan and Friedman demonstrated that a simple Hamiltonian model for a lattice of interacting magnetic spins could be adapted to capture the phenomenology of the ocular dominance and orientation maps (Cowan and Friedman 1991). Magnetic lattice models derive from the classical Ising and XY spin models. In the Ising model each site of a lattice $\{i \in \mathbb{Z}_N^2\}$ has a spin that can be "up" ($z_i = +1$) or "down" ($z_i = -1$). Each pair of neighboring sites $\langle i, j\rangle$ contributes an amount $J_{ij} z_i z_j$ to the total energy. In addition, an external magnetic field h_i may be applied to site i. The energy is given by the Hamiltonian function $H[\mathbf{z}] = -\frac{1}{2}\sum_{ij} J_{ij} z_i z_j + \sum_i h_i z_i$, where $\mathbf{z}$ denotes a particular configuration of all the z_i. Classically, J_{ij} is one when i and j are adjacent and zero otherwise. Taking into account the effective form of locally excitatory, laterally inhibitory cortico-cortical interactions Cowan and Friedman (1991) introduced a spatially extended Ising model by replacing J_{ij} with a new coupling function

$$A_{ij} = g(i - j, \sigma_+^2) - g(i - j, \sigma_-^2), \tag{1}$$

where g represents a Gaussian $g(u, \sigma^2) = \exp[-(|u|/\sigma)^2/2]/(2\pi\sigma^2)^{d/2}$, and $\sigma_- \approx 3\sigma_+$, and $d = 1$ or 2 depending on the dimensionality of the argument $u \in \mathbb{R}^d$. In thermal equilibrium, at a given inverse temperature $\beta = 1/kT$, any one of the $2^{(N^2)}$ possible spin configurations $\mathbf{z}$ occurs with probability given by the Gibbs distribution $P(\mathbf{z}) = \exp(-\beta H[\mathbf{z}])/Z(\beta)$, where $Z(\beta)$ is the partition function $Z(\beta) = \sum_{\mathbf{z}} \exp(-\beta H[\mathbf{z}])$. At low temperatures ($\beta \gg 1$) the system approaches a state in which all spins are coaligned (for $h_i \equiv 0$), corresponding to maximal magnetization. As β is reduced, nearly optimal energy states—those with relatively small numbers of misaligned spins—grow in probability relative to the pure $+1$ or -1 state. At high

temperature ($\beta \ll 1$) the highly disordered states, with no correlation between neighboring spins, predominate. At the extreme of $\beta \to 0$, all configurations have the same probability $2^{-(N^2)}$. As β increases from zero, correlations begin to appear between nearby spins. At a critical temperature β_c the classical Ising model exhibits a phase transition at which the correlation length diverges and beyond which the spontaneous magnetization is nonzero. Analogous behavior has been observed for the spatially extended Cowan–Friedman model (Thomas 2000).

In the closely related XY model, the binary spins z_i are replaced by planar unit vectors $\chi_i = \begin{pmatrix} \cos\theta_i \\ \sin\theta_i \end{pmatrix}$ that interact according to the Hamiltonian

$$H[\underline{\chi}] = \sum_{ij} J_{ij}\chi_i \cdot \chi_j = \sum_{ij} J_{ij}\cos(\theta_i - \theta_j). \tag{2}$$

Unlike the Ising model, the XY model does not exhibit spontaneous magnetization (alignment of the spins) even as $\beta \to 0$ because the θ_i are continuously variable (Cardy 1996; Kosterlitz and Thouless 1978; Mermin and Wagner 1966). A point about which path integration of $\nabla\theta(x)$ gives $\pm 2k\pi$ is a *vortex* or a *spin singularity* of degree $\pm k$ (see Fig. 1). The system develops vortex-antivortex pairs which are stable even at low temperatures. As the temperature increases, the phase transition occurs through the unbinding of vortex pairs; at high temperature the correlation length drops as in the Ising model. Representative equilibrium configurations from the Gibbs distribution at a given temperature may be obtained by Monte Carlo sampling techniques such as the Metropolis–Hastings algorithm (Glauber 1963; Hastings 1970; Metropolis et al. 1953) [see (Binder and Heermann (1997); Thomas (2000)) for details]. For low temperatures the system approximately descends the gradient of the Hamiltonian, leading to the following update rule $\theta_k \to (\theta_k + \Delta\theta_k) \mod \pi$:

$$\Delta\theta_k \approx -\eta\frac{\partial H[\underline{\theta}]}{\partial\theta_k} = -\eta\frac{\partial}{\partial\theta_k}\frac{-1}{2}\sum_{ij} J_{ij}\cos(\theta_i - \theta_j) = -\eta\sum_j J_{kj}\sin(\theta_k - \theta_j), \tag{3}$$

where η is an effective rate constant. The system will dwell for long times in metastable states characterized by $\sum_j J_{ij}\sin(\theta_i - \theta_j) = 0, \forall i \in \mathbb{Z}_N^2$. Cowan and Friedman (1991) showed that replacing the classical nearest-neighbor XY interaction J_{ij} with the spatially extended center-surround interaction A_{ij} generated reasonable simulacra of orientation maps observed through optical imaging. Figure 1 shows examples of metastable distributions for the classical ferromagnetic and spatially extended mixed ferro-/antiferromagnetic coupling interactions.

3 Hebbian plasticity and geometry of thalamocortical weights

Following Thomas and Cowan (2006) we caricature the cortical map as arising from feedforward connections from an input layer to an output layer, as illustrated in Fig. 2. We further approximate the output-layer activity as a linear filter of the input layer

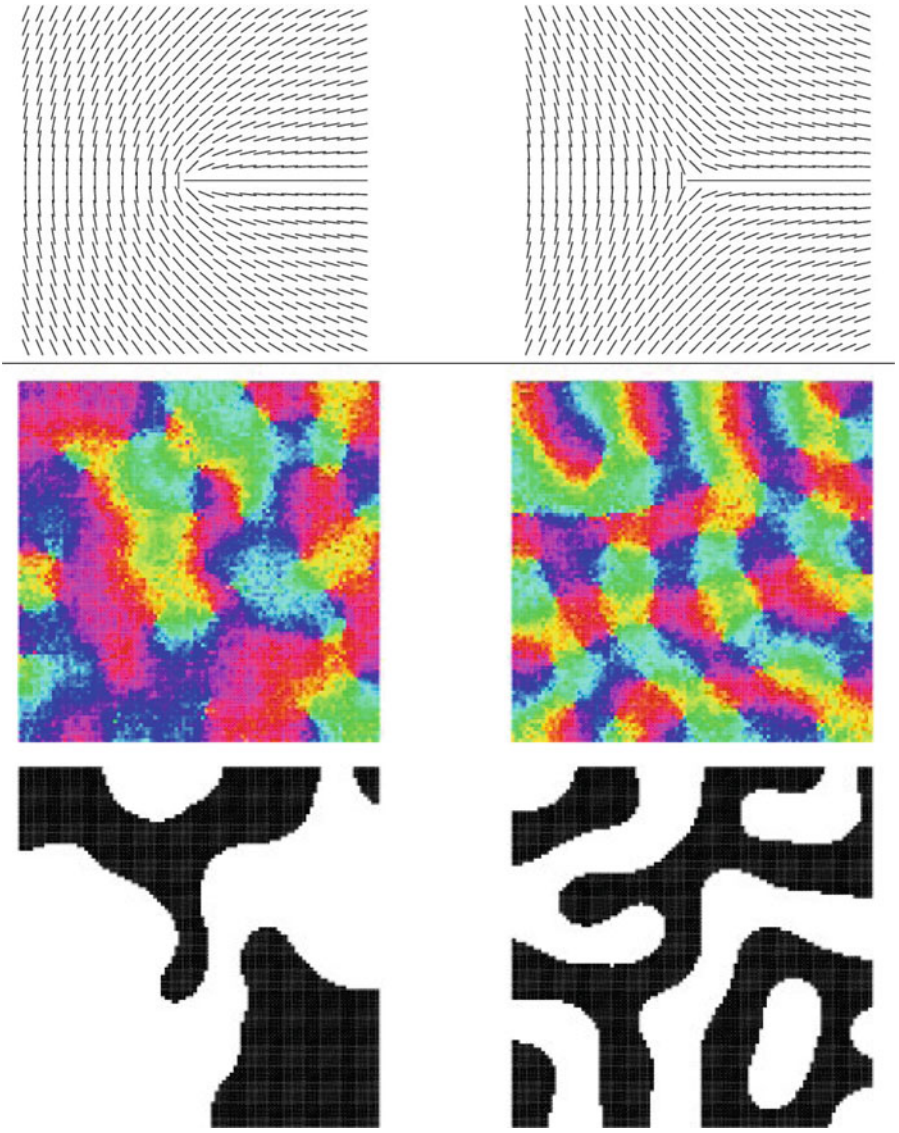

Fig. 1 *Top* Topological point defects in a π–periodic orientation variable $\phi(x)$. *Left* $+1$. *Right* -1. Both defect patterns approach local constancy as $|x| \to \infty$. *Middle and bottom* Examples of Ising and XY patterns. Sample patterns generated by the Ising and XY Models with ferromagnetic interaction J_{ij} and center-surround interaction A_{ij} on 100×100 grids with zero-flux boundary conditions. *Middle* XY models. *Bottom* Ising models. *Left* $J_{ij} = g(|i-j|, (60\mu)^2)$. *Right* $A_{ij} = g(|i-j|, (100\mu)^2) - g(|i-j|, (300\mu)^2)$. *Box size* 2 mm

activity. We change the feedforward synaptic weights according to a linear correlation-based rule, with the addition of nonlinear additive constraints to saturate synaptic growth. As a first model for the feedforward weights we combine On-center, Off-center, lagged and nonlagged connections, etc., into an aggregate feedforward

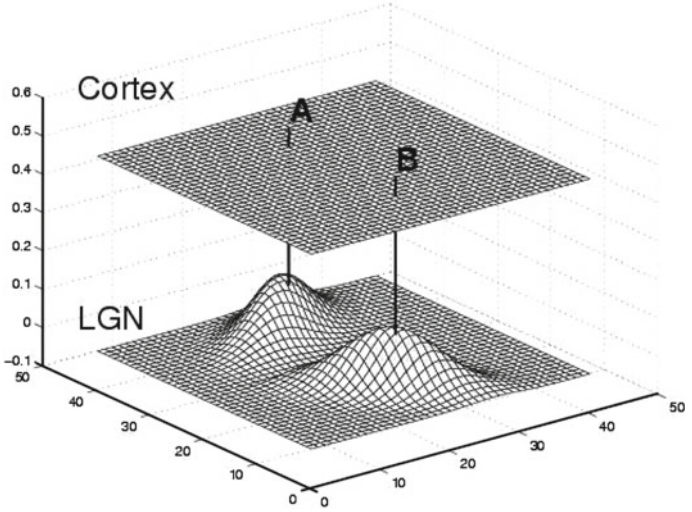

Fig. 2 Feed-forward weights from the input layer to the output layer (labeled "LGN" and "Cortex" respectively). Shown are $w(x, r)$ for two different locations in the cortex, $x = A$ and $x = B$. The weight distributions shown are Gaussian ellipsoids with major axes oriented at angles of $\pi/6$ (A) and $3\pi/4$ (B). We will interpret the center-of-mass of each distribution as the retinotopy associated with output-layer location A or B; likewise the eccentricity and orientation of the ellipses will determine the the orientation tuning and orientation preference of the cortex at A and B. Reproduced, with permission, from Thomas and Cowan (2006)

weight. We take the cell's receptive-field properties such as spatial position and orientation to be determined by the geometry of the feedforward synaptic weight.

We illustrate how the reduction works for a monocular model, in which the moments of the aggregate afferent synaptic weight distribution yield the maps for the net input weight or "fan-in", the retinotopic map, the orientation-tuning vector map and a map of receptive-field size.

We imagine a succession of activity patterns in the (two-dimensional) input layer, $I(r)$, that lead to activities $a(x)$ in the output layer determined by the feedforward weights $w(x, r)$ and a fixed isotropic lateral interaction $A(x)$, such as a center-positive difference of Gaussians. Denoting the feedforward input as $I_{\mathrm{ff}}(x) = \int_{r'} w(x, r')I(r')\,dr'$, and the resulting cortical (output-layer) activity $a(x) = \int_{x'} A(x - x')I_{\mathrm{ff}}(x')\,dx$ (after some relaxation time short compared to the inverse of the relevant learning rate η) we arrive at an effective linear-filter approximation for the output layer activity (Wimbauer et al. 1998)

$$a(x) = \int_{x'} A(x - x') \int_{r'} w(x', r')I(r')\,dr'. \tag{4}$$

The mechanism of Hebbian learning specifies a rule for modifying synaptic weights based on the correlation of pre- and post-synaptic activity. In its simplest form, the changes in the weights are directly proportional to the correlations:

$$\Delta w(x, r) = \eta\langle I(r)a(x)\rangle. \tag{5}$$

The Hebb rule update of $w(x, r)$ depends on the correlation function $\langle I(r)a(x)\rangle$, which is given by

$$\langle I(r)a(x)\rangle = \int_{x'} A(x - x') \int_{r'} \langle I(r)I(r')\rangle w(x', r')\, dr'\, dx'. \tag{6}$$

It is natural to assume that the auto-correlation function $C(r, r')$ of the inputs is invariant under translations $r \to r + r_0$, reflections $r \to -r$ and rotations $r \to \mathrm{Rot}_\theta r$. Let $C(r - r') = \langle I(r)I(r')\rangle$ denote such a correlation function. Then the update rule (5) becomes a double convolution

$$\Delta w(x, r) = \eta \int_{x'} A(x - x') \int_{r'} C(r - r')w(x', r')\, dr'\, dx'. \tag{7}$$

The learning rate η is taken to be small enough that the weight changes are based on the entire ensemble of input patterns $I(r)$ rather than being driven by a small number of them. We take this time-averaged input–output correlation, with linear weight decay, for our basic learning rule $\mathbf{F}_0[w]$. The learning rule is unconstrained in the sense that we do not (yet) impose restraints on the net efferent or afferent weights (cf. Eq. 12). We do, however, require $w(x, r) \geq 0$, so our rule is in fact semi-unconstrained. Leaving the time-dependence of the weights implicit, we write the basic learning-rule:

$$\begin{aligned} \frac{d}{dt} w(x, r) &= \mathbf{F}_0[w](x, r) = \eta \mathbf{E}[a(x)I(r)] - \alpha w(x, r) \\ &= \eta \int_{x'} A(x - x') \int_{r'} C(r - r')w(x', r')\, dr' - \alpha w(x, r) \end{aligned} \tag{8}$$

$$w(x, r) \geq 0. \tag{9}$$

We use η to denote the (slow) feedforward learning-rate; $\mathbf{E}[\cdots]$ represents the expected value, and α represents an intrinsic synaptic weight decay rate. We assume that the correlation function of activity in the input layer, $\mathbf{E}[I(r')I(r)] = C(r - r')$, is isotropic and translation-invariant.

Constraints on synaptic weight have been shown to influence pattern formation in models of ocular dominance column development (Miller and MacKay 1994). In Thomas and Cowan (2006), it was shown that imposing simultaneous uniformity constraints on the net synaptic weight diverging from each point in the input layer, and the net synaptic weight converging to each point in the output layer, and imposing a uniform retinotopic map constraint, together were inconsistent with elongated receptive fields representing different orientation preferences. Instead of imposing hard a priori upper limits on the fan-in or fan-out, we will supplement the linear growth rule (8) to include "soft" nonlinear constraints limiting growth of the synaptic weights. Here we assume that limits to the physical size of dendritic arbors and the packing density of afferent fibers, and limitations to the amount of stimulation a cell can tolerate, prevent the net feedforward input or *fan-in* $\lambda(x)$ at a given cortical location,

$$\text{人}(x) = \int_r w(x,r)\,dr, \tag{10}$$

from growing without bound. We assume that the fan-in $\text{人}(x)$ tends towards an equilibrium level of input weight 人_0 at each cortical location, through an unspecified homeostatic mechanism.[3]

Similarly, physiological and geometric constraints limit the amount of outgoing synaptic weight that a given input-layer (e.g. geniculate) cell can project to the cortex. The net output weight or *fan-out* $\Upsilon(r)$, given by

$$\Upsilon(r) = \int_x w(x,r)\,dx, \tag{11}$$

also tends toward a preferred level consistent with the retinocortical magnification μ (mm CTX/mm LGN), i.e. $\Upsilon_0 = \mu^2 \text{人}_0$. We model these uniformity constraints in both $\text{人}(x)$ and $\Upsilon(r)$ with logistic growth terms, modifying the unconstrained learning-rule to read:

$$\begin{aligned}\frac{d}{dt}w(x,r) &= \mathbf{F}[w](x,r) = \mathbf{F}_0[w](x,r) + \mathbf{F}_{\text{constr}}[w](x,r)\\ &= \eta \int_{x'} A(x-x') \int_{r'} C(r-r')w(x',r')\,dr'\,dx' - \alpha w(x,r) \qquad (12)\\ &\quad + w(x,r)\{c_{\text{人}}(\text{人}_0 - \text{人}(x)) + c_\Upsilon(\Upsilon_0 - \Upsilon(r))\};\\ w(x,r) &\geq 0. \qquad (13)\end{aligned}$$

Equation 12 is our high-dimensional description of the developmental dynamics. We keep the hard lower limit of nonnegative synaptic weights (Eq. 13).

Given a model for the development of the feedforward weights $w(x,r)$, we define developmental rules for cortical maps of orientation, retinotopy, etc. in terms of the lowest order moments of w. Table 1 summarizes the definitions used in Thomas and Cowan (2006): the net fan-in of synaptic weight to location x, $\text{人}(x)$, is the zeroth moment (in r) of $w(x,r)$; the retinotopic map vector, $R(x)$, is given by the first moment or center-of-mass; and the receptive-field width and orientation tuning vector are determined by the 2×2 matrix of second moments. In this way we derive developmental rules for low dimensional maps directly from the high dimensional dynamics of Eqs. 12 and 13.

The covariance matrix $Q(x)$ is the 2×2 symmetric matrix obtained from the second moments of the synaptic weight afferent to x about its center of mass, $R(x)$. Any such matrix can be represented as the sum of its trace and a symmetric traceless matrix, i.e. $Q = \text{Trace}[Q]I_2 + q[Q]\Phi_2(\phi[Q])$, where $\Phi_2(\phi) = \begin{pmatrix}\cos(2\phi) & \sin(2\phi)\\ \sin(2\phi) & -\cos(2\phi)\end{pmatrix}$, I_2 is

[3] For perspectives on models of such competitive homeostatic mechanisms see Elliott and Shadbolt (2002); Song et al. (2000).

Table 1 Geometrical reduction of synaptic weight $w(x, r)$

Quantity	Definition	Interpretation
$\lambda(x)$	$\int_r w(x, r)\, dr$	Fan-in (input mass)
$R(x)$	$\frac{1}{\lambda(x)} \int_r w(x, r) r\, dr$	Retinotopy vector
$Q(x)$	$\frac{1}{\lambda(x)} \int_u w(x, u + R(x)) u u^T\, du$	Covariance matrix
$\sigma(x)$	$\sqrt{\text{Trace}[Q(x)]}$	Receptive field width
$q(x)$	$\sqrt{(Q_{11} - Q_{22})^2 + (2Q_{12})^2}$	Orientation selectivity
$\phi(x)$	$\frac{1}{2} \tan^{-1}\left(\frac{2Q_{12}}{Q_{11} - Q_{22}}\right)$	Preferred orientation

The zeroth and first moments of the receptive field at x, $w(x, r)$, define the input mass (fan-in) and the retinotopy (center-of-mass). The planar vector $u = r - R(x)$ captures the displacement of a point r, in the geniculate, from the center of mass $R(x)$ associated with cortical location x. The 2×2 symmetric matrix of second moments $Q(x)$ defines the receptive field width, preferred orientation, and orientation tuning strength

the 2×2 identity matrix, $q[Q] = \sqrt{\text{Trace}[Q]^2 - 4 \det[Q]}$ represents the orientation selectivity due to elongation of the weight profile, and the preferred orientation is given by the direction of elongation of the receptive field,

$$\phi[Q] = \frac{1}{2} \tan^{-1}\left(\frac{2Q_{12}}{Q_{11} - Q_{22}}\right). \tag{14}$$

The width of the receptive field is captured by $\sigma(x) = \sqrt{Q_{11}(x) + Q_{22}(x)}$.

The planar Gaussian distribution with the same covariance matrix,

$$g(u, Q) = \frac{1}{2\pi\sqrt{\det[Q]}} \exp\left[-\frac{1}{2} u^T Q^{-1} u\right] \quad (u \in \mathbb{R}^2), \tag{15}$$

has elliptical level curves with major axis in the direction $\phi[Q]$, and a major-to-minor axis ratio AR satisfying $q = \left(\frac{\text{AR}^2 - 1}{\text{AR}^2 + 1}\right) \sigma^2$. We define the orientation preference vector χ associated with a covariance matrix Q to be

$$\chi = q \begin{bmatrix} \cos(2\phi) \\ \sin(2\phi) \end{bmatrix} = \begin{bmatrix} Q_{11} - Q_{22} \\ 2Q_{12} \end{bmatrix}. \tag{16}$$

The magnitude of this vector ranges between 0 and $\sigma^2 = \text{Trace}[Q]$. When $q = 0$, Q is a multiple of the identity matrix, and $g(u, Q)$ becomes a circularly-symmetric planar Gaussian with standard deviation σ. As q increases, the eccentricity of the ellipses increases from zero to a maximum equal to the trace of Q. The vector χ is invariant under π-fold rotation of the plane, or $u \to -u$. The subsequent analysis is made possible by the fact that the components of χ are linear combinations of the second moments of the incoming weight distribution (the Q_{ij}). When the net fan-in is uniform ($\lambda(x)$ is constant), then $\chi(x)$ is a linear functional of the synaptic weight $w(x, r)$, because the matrix elements of $Q(x)$ are themselves linear functionals of the synaptic weight.

4 Reduction from high-dimensional to low-dimensional dynamics by linearization about a homogeneous steady state

Our strategy for studying the development of anisotropic structure in the feedforward connections is to identify a homogeneous, isotropic steady-state that is stable for some range of parameters, and then to study the linearized dynamics near loss of stability of the isotropic steady state.

4.1 Homogeneous steady-state

The retinocortical magnification μ varies significantly from the foveal to the peripheral region of the visual field. For the purposes of studying local emergence of cortical map patterns, however, we may consider μ to be constant within the domain of interest. Moreover, without loss of generality we may choose units for the retinotopic coordinate r and the cortical coordinate x so that $\mu = 1$. If a uniform, isotropic steady-state exists, it then has the form $w(x, r) = f(x - r)$ for some nonnegative, circularly symmetric function f. If w has this form, then it is easy to show that the integral

$$\mathscr{I}(x, r) = \int_{x'} \int_{r'} A(x - x')C(r - r')f(x' - r')\,dr'\,dx' \tag{17}$$

is translation invariant in the sense that for any $y \in \mathbb{R}^2$, $\mathscr{I}(x + y, r + y) = \mathscr{I}(x, r)$, or equivalently $\mathscr{I}(x, r) = I(x - r)$. It is also straightforward to show that when w is uniform and isotropic that $I(x - r)$ takes the form of a single variable convolution. Writing $u = x - r$ and $u' = x' - r'$ for the deviation of r from the center of mass of the homogeneous distribution[4] we have

$$I(u) = \int_{u' \in \mathbb{R}^2} L(u - u')f(u')\,du' \tag{18}$$

where $L(u) = \int_{u' \in \mathbb{R}^2} A(u - u')C(u')\,du'$ is the resulting one variable integral kernel. Consequently, existence of an isotropic steady state solution to Eqs. 12 and 13 is equivalent to existence of a solution to the nonlinear eigenvalue problem

$$f(u) = c\left[\int_{u' \in \mathbb{R}^2} L(u - u')f(u')\,du'\right]_+, \tag{19}$$

where $[v]_+ = \max(v, 0)$ and c is an eigenvalue. To see this, note that when w is uniform, the fanin $\curlywedge(x)$ and fanout $\curlyvee(r)$ are both constant, reducing the last term in Eq. 12 to $w(x, r)(k_1 + k_2)$, for $k_1 = c_{\curlywedge}(\curlywedge_0 - \curlywedge)$ and $k_2 = c_{\curlyvee}(\curlyvee_0 - \curlyvee)$. Together with

[4] Without loss of generality we may assume that f is centered, i.e. $\int_{u \in \mathbb{R}^2} f(u)u\,du = 0$ so $u = 0$ is the center of mass of $f(u)$.

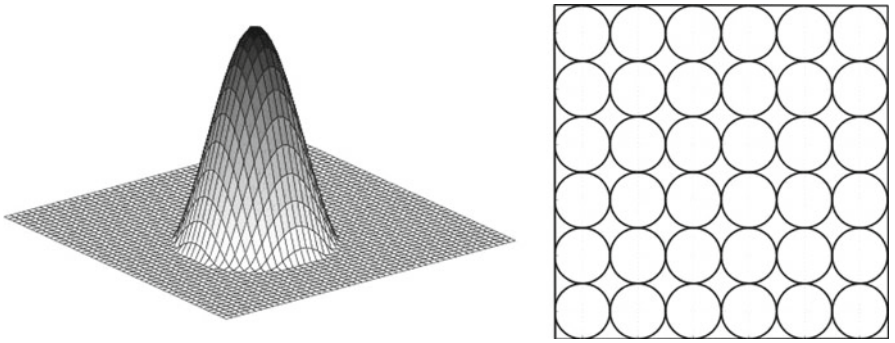

Fig. 3 Constrained receptive-field dynamics and steady-state. *Left* Steady-state shape of a single receptive field for Eq. 12, determined numerically. The shape is approximately that of a circularly-symmetric Gaussian, smooth except where w becomes zero. *Right* Uniform retinotopy of steady-state solution. The rings represent the receptive fields in retinotopic (input-layer) coordinates of cells sampled from a regular grid on the cortex (output-layer)

the linear decay term we see that the eigenvalue must satisfy $c = 1/(k_1 + k_2 - \alpha)$. The eigenvalue problem is nonlinear both because of the rectifying nonlinearity $[\cdot]_+$ and because c depends nonlinearly on f, through k_1, k_2. Numerically, it is straightforward to set up an iterative scheme that converges to an approximate solution of Eq. 19. Figure 3 shows a steady-state receptive field for the uniform solution, as well as the arrangement of retinotopy for a regular array of output-layer (cortical) loci.

The uniform steady state will be stable for sufficiently large values of the weight-decay parameter α. As α is reduced we uncover pattern-formation at the largest eigenvalue of the linear system given by linearizing the dynamical system of Eq. 12 about the steady state. Certain perturbations of the uniform weight pattern begin to grow, disturbing the circularly-symmetric receptive fields, creating nonzero preferences for orientation, and inhomogeneities in retinotopic location of receptive-field centers. We proceed by examining the evolution of weight patterns that begin as small deviations from the uniform steady-state. We discard all information about the receptive field structure except that contained in the moments in Table 1, and derive dynamical update rules for those moments and their interactions.

The moments of interest form a cortical map vector $\mathbf{v}(x)$ defined so that $\mathbf{v} = \mathbf{0}$ in the uniform steady-state (see Table 2). The components of $\mathbf{v}$ are related mutatis mutandis to the receptive field moments given in Table 1:

1. $\hat{\lambda}(x) = \lambda(x) - \lambda_{\mathrm{SS}}$, the deviation of the net input weight from its uniform steady-state value;

2–3. $s(x) = R(x) - x/\mu$ (two components), the deviation of the retinotopic map from its uniform value;

4–5. $\chi(x)$ (two components), the orientation preference vector; and

6. $\rho(x) = \sigma^2(x) - \sigma_{ss}^2$, the deviation of the squared receptive-field width from the uniform steady-state value.

Deviations of $w(x, r)$ about its steady-state configuration will result in deviation of $\mathbf{v}(x)$ away from zero. Because these moments are linear functionals of the synaptic

Table 2 Cortical map vector components derived from linearization of the high-dimensional dynamics about a fixed point corresponding to uniform, isotropic retinotopy and receptive field structure

Map component	Definition	Name
$\hat{\lambda}(x)$	$\lambda(x) - \lambda_0$	Input weight deviation
$s(x)$	$R(x) - \frac{x}{\mu}$	Retinotopic distortion vector
$\chi(x)$	$\begin{pmatrix} Q_{11}(x) - Q_{22}(x) \\ 2Q_{12}(x) \end{pmatrix}$	Orientation tuning vector
$\rho(x)$	$\sigma^2(x) - \sigma_0^2$	R.F. width deviation

See Table 1 for definitions of λ (fan-in), R (retinotopy), and Q (quadratic form of second moments)

weight function, the linear dynamics of $\mathbf{v}(x)$ is given by the corresponding moments of the linearization of the constrained dynamics in Eq. 12 about the steady-state.

4.2 Derivation of linear interactions between cortical map components, part I

In the homogeneous steady state shown in Fig. 3 the receptive fields have uniform fan-in weight

$$\frac{\hat{\lambda}(x)}{\lambda_0} = \frac{\lambda(x) - \lambda_0}{\lambda_0} = 0, \tag{20}$$

regular retinotopy

$$s(x) = R(x) - \frac{x}{\mu} = 0, \tag{21}$$

circularly symmetrical profiles

$$\chi(x) = \begin{pmatrix} Q_{11} - Q_{22} \\ 2Q_{12} \end{pmatrix} = 0, \tag{22}$$

and uniform widths

$$\rho(x) = \sigma^2(x) - \sigma_0^2 = 0. \tag{23}$$

Thus the cortical-map vector for the homogeneous Gaussian state is identically zero:

$$\mathbf{v} = \left(\frac{\hat{\lambda}(x)}{\lambda_0}, s_1(x), s_2(x), \chi_1(x), \chi_2(x), \rho(x) \right) \equiv \mathbf{0}. \tag{24}$$

For clarity, we retain the geniculocortical magnification factor μ.

In order to linearize about the steady-state, we approximate the receptive-field profile shown in Fig. 3 with $w_0(x, r)$, a Gaussian profile with the same net fan-in,

center-of-mass and covariance matrix:

$$w_0(x,r) = \frac{\curlywedge(x)}{2\pi\sqrt{\det[Q]}} \exp\left[-\frac{1}{2}u^T Q^{-1}(x)u\right] \tag{25}$$

$$u = R(x) + r. \tag{26}$$

This approximation is acceptable as long as the information in third or higher moments does not compromise our linear description of the dynamics of the zeroth through second moments of $w(x,r)$.

The dynamical behavior of each cortical map "feature" is described by the corresponding moment of Eq. 12 (see Table 1 for the moment definitions):

$$\frac{d}{dt}\hat{\curlywedge}(x) = \int_{r\in\mathbb{R}^2} \eta(\mathbf{F}[w](x,r))\,dr \tag{27}$$

$$\frac{d}{dt}(\curlywedge(x)s(x)) = \int_{r\in\mathbb{R}^2} \eta(\mathbf{F}[w](x,r))\left(r - \frac{x}{\mu}\right)dr \tag{28}$$

$$\frac{d}{dt}(\curlywedge(x)\chi(x)) = \int_{u\in\mathbb{R}^2} \eta(\mathbf{F}[w](x,u+R(x)))\begin{pmatrix} u_1^2 - u_2^2 \\ 2u_1u_2 \end{pmatrix} du \tag{29}$$

$$\frac{d}{dt}(\curlywedge(x)\rho(x)) = \int_{u\in\mathbb{R}^2} \eta(\mathbf{F}[w](x,u+R(x)))\frac{||u||^2}{2}\,du \tag{30}$$

Note that the retinotopy $R(x) = s(x) + x/\mu$ includes the (small) retinotopic distortion vector field $s(x)$.

There is a cascade of perturbation effects from lower moments to higher moments. Inhomogeneities in $\curlywedge(x)$ affect all the higher moment, as evident in Eqs. 27–30. Inhomogeneities in the retinotopy vector $s(x)$ affect the dynamics of the orientation vector and the receptive field width.

The dynamical constraints on weight evolution include a logistic constraint on the net fan-out weight $\curlyvee(r)$ from each input-layer location r. In the homogeneous state the fan-out has a uniform value $\curlyvee_0 = \mu^2\curlywedge_0$, or $\curlyvee_0 = \curlywedge_0$ if we choose choose units in which the thalamocortical magnification factor $\mu = 1$. Variation of the fan-in weight, the centers of the receptive fields, or their elongation in various directions, disturb the uniformity of the fan-out, inducing a perturbation $\hat{\curlyvee}(r) = \curlyvee(r) - \curlyvee_0$. For example, if the receptive fields of two nearby cortical cells move their centers closer together than would be dictated by the homogeneous spacing $|\Delta r| = |\Delta x|/\mu$, the input-layer locations in the region of increased overlap gain net fan-out weight while those just beyond the original cell centers lose net fan-out weight. In this way the uniform coverage of all input-layer locations becomes compromised, so the logistic $\curlyvee$-term provides reinforcement of the homogeneous state. The consequences of strict constraints on fan in and fan out were explored systematically in Thomas and Cowan (2006), in the absence of a specific learning rule.

It will be shown (Sect. 4.4) that a linearized perturbation analysis of simultaneous pattern formation near the uniform isotropic steady state, using the moment evolution Eqs. 27–30 leads to a generalized spin model of the form

$$\frac{1}{\eta}\frac{d}{dt}\mathbf{v} = -\alpha\mathbf{v} + \lambda A * \mathbf{v} + \mathbf{K} * \mathbf{v} \tag{31}$$

where $*$ denotes the convolution operator, A is a difference-of-Gaussians center-surround coupling, $\mathbf{K}$ is a six-by-six matrix of convolution kernels K_{ij}, and

$$(\mathbf{K} * \mathbf{v})_i := \sum_{j=1}^{6} \left(\int_{x' \in \mathbb{R}^2} K_{ij}(x - x')\mathbf{v}_j(x')\, dx' \right). \tag{32}$$

The fact that each component of the retinotopic map vector $\mathbf{v}$ is convolved with the same coupling interaction A means that all map components begin to form patterns at a common underlying wavelength. This result is exploited to account for observed coupling between cortical map components in Thomas and Cowan (2004). The calculation for the full system is somewhat technical. Before embarking upon it, we illustrate the main ideas in a simpler special case in the next section. The general case is treated in Sect. 4.4.

4.3 Orientation map development with other maps fixed

As a special case of the method summarized above, it is instructive to consider the combined effects of Hebbian learning and center-surround cortical interaction on the development of a single map element, the orientation preference map. The derivation of the full model is provided in Sect. 4.4. If we restrict the evolution of the synaptic weights $w(x, r)$ by allowing orientation preferences to vary while keeping the net input weight $\lambda(x)$, the retinotopic map $R(x)$ and the receptive field widths $\sigma(x)$ fixed to their uniform values, we recover the XY spin model for the orientation preference vector $\chi(x)$, as we now demonstrate.

Assume that the input mass and retinotopy are uniform, i.e. $\lambda(x) = \lambda_0$ and $R(x) = R_0 + (x - x_0)/\mu$. The effect of a small change Δw in the weights on the orientation at x is felt through the changes in the elements of the covariance matrix ΔQ_{ij}. Differentiating Eq. 14 gives

$$2\Delta\phi(x) = \left(\frac{\cos(2(\phi(x) + \frac{\pi}{2}))2\Delta Q_{12}(x) - \sin(2(\phi(x) + \frac{\pi}{2}))(\Delta Q_{11} - \Delta Q_{22})}{q(x)} \right). \tag{33}$$

The changes induced in Q by a change Δw due to the unconstrained learning rule (ignoring weight decay, which does not affect receptive field shape) are found by taking the second moments of Eq. 7 in the plane:

$$\begin{aligned}\Delta Q(x) &= \frac{1}{\lambda_0}\int_u uu^T \Delta w(x, u + R(x))\, du \\ &= \frac{\eta}{\lambda_0}\int_u uu^T \int_{x'} A(x - x') \int_{r'} C(u + R(x) - r')w(x', r')\, dr'\, dx'\, du \\ &= \frac{\eta}{\lambda_0}\int_{x'} A(x-x') \int_{r'} w(x', r') \int_u uu^T C(u+R(x)-r')\, du\, dr'\, dx'. \end{aligned} \tag{34}$$

In addition to being symmetric under translation, rotation and reflection, we take the input layer correlation function C to be normalized, i.e. $\int_r C(r)\, dr = 1$. This may be arranged by changing the constant η if necessary. Together with the symmetry of C this condition guarantees the center-of-mass of C is at 0:

$$\int_u C(u + v)u\, du = -v. \tag{35}$$

Exploiting Eq. 35 we can calculate the inner integral:

$$\begin{aligned}&\int_u uu^T C(u + R(x) - r')\, du \\ &= \int_u ((u + R(x) - r')(u + R(x) - r')^T - u(R(x) - r')^T \\ &\quad - (R(x) - r')u^T - (R(x) - r')(R(x) - r')^T)C(u + R(x) - r')\, du \\ &= \sigma_C^2 I_2 + (R(x) - r')(R(x) - r')^T \end{aligned} \tag{36}$$

where σ_C is the width of C. Similarly, the center of mass of $w(x', r')$ is $R(x')$. Denoting the difference in retinotopy, $R(x) - R(x')$, by ΔR, we find

$$\begin{aligned}&\int_{r'} w(x', r') \int_u uu^T C(u + R(x) - r')\, du\, dr' \\ &= \int_{r'} \frac{w(x', r')}{\lambda_0}(\sigma_C^2 I_2 + (R(x) - r')(R(x) - r')^T)\, dr' \\ &= \sigma_C^2 I_2 + \int_{r'} \frac{w(x', r')}{\lambda_0}(\Delta R + R(x') - r')(\Delta R + R(x') - r')^T\, dr' \\ &= \sigma_C^2 I_2 + \int_{r'} \frac{w(x', r')}{\lambda_0}(\Delta R \Delta R^T + \Delta R(R(x') - r')^T \\ &\quad + (R(x') - r')\Delta R^T + (R(x') - r')(R(x') - r')^T)\, dr' \\ &= \sigma_C^2 I_2 + \Delta R \Delta R^T + Q(x') \\ &= \sigma_C^2 I_2 + \frac{1}{\mu^2}(x - x')(x - x')^T + Q(x') \end{aligned} \tag{37}$$

If we assume that C is a two-dimensional Gaussian with width σ_C and A is a difference of Gaussians as in Eq. 1, we can now complete the outer integral in Eq. 34:

$$\begin{aligned}
&\int_{x'} A(x-x') \int_{r'} w(x',r') \int_{u} uu^T C(u+R(x)-r')\,du\,dr'\,dx' \\
&\quad = \text{人}_0 \int_{x'} A(x-x') \left(\sigma_C^2 I_2 + \frac{1}{\mu^2}(x-x')(x-x')^T + Q(x')\right) dx' \\
&\quad = \text{人}_0 \left(\frac{1}{\mu^2}\int_{y} yy^T A(y)\,dy + \int_{x'} A(x-x')Q(x')\,dx'\right) \\
&\quad = \frac{\text{人}_0}{\mu^2}(\sigma_+^2 - \sigma_-^2) I_2 + \text{人}_0 \int_{x'} A(x-x')Q(x')\,dx'. \qquad (38)
\end{aligned}$$

Note that σ_+ (respectively, σ_-) is the width of the narrow positive (respectively, broad negative) Gaussian contributing to the center-surround interaction A. Thus the update rule for the elements of $Q(x)$ is given by

$$\Delta Q(x) = \eta \left(\frac{\sigma_+^2 - \sigma_-^2}{\mu^2} I_2 + \int_{x'} A(x-x')Q(x')\,dx'\right). \qquad (39)$$

In terms of the quantities in Eq. 33 we can write

$$\Delta(Q_{11} - Q_{12})(x) = \eta A * (Q_{11} - Q_{22}) = \eta A * \left(q(x)\cos 2\left(\phi(x) + \frac{\pi}{2}\right)\right) \qquad (40)$$

$$2\Delta Q_{12}(x) = \eta A * (2Q_{12}) = \eta A * \left(q(x)\sin 2\left(\phi(x) + \frac{\pi}{2}\right)\right) \qquad (41)$$

where the notation $(f * g)(x) = \int_{x'} f(x-x')g(x')\,dx'$ again denotes convolution. If we take our orientation "spin" vectors to have uniform magnitude $q(x) = q_0$ as in the classical XY model, we have

$$\begin{aligned}
&2\Delta\phi(x) \\
&= \eta \frac{q_0\left(\cos 2\left(\phi(x)+\frac{\pi}{2}\right) A * \sin 2\left(\phi(x)+\frac{\pi}{2}\right) - \sin 2\left(\phi(x)+\frac{\pi}{2}\right) A * \cos 2\left(\phi(x)+\frac{\pi}{2}\right)\right)}{q_0} \\
&= \eta \int_{x'} A(x-x') \\
&\quad \times \left[\cos 2\left(\phi(x)+\frac{\pi}{2}\right)\sin 2\left(\phi(x')+\frac{\pi}{2}\right) - \sin 2\left(\phi(x)+\frac{\pi}{2}\right)\cos 2\left(\phi(x')+\frac{\pi}{2}\right)\right] dx' \\
&= \eta \int_{x'} A(x-x')\sin(\phi(x') - \phi(x))\,dx' \qquad (42)
\end{aligned}$$

which is the low-temperature XY update rule given by Eq. 3.

4.4 Derivation of linear interactions between cortical map components, part II

In the homogeneous steady state, which we approximate by the Gaussian weight distribution

$$w_0(x,r) = \lambda_0 g\left(\frac{x}{\mu} - r, \sigma_0^2\right) := \frac{\lambda_0}{2\pi\sigma_0^2}\exp\left(-\frac{|\frac{x}{\mu} - r|^2}{2\sigma_0^2}\right),$$

the receptive fields are assumed to have uniform fan-in weight, regular retinotopy, circularly symmetrical profiles, and uniform widths. Thus the cortical-map vector $\mathbf{v} \equiv \mathbf{0}$, for the homogeneous Gaussian state (Eq. 24).

Rather than study the linearization of Eq. 12 about $w_0(x,r)$ with respect to arbitrary perturbations $w_0(x,r) + \varepsilon h(x,r)$, we restrict attention to the geometrical properties of a perturbation $h(x,r)$ corresponding to the cortical maps of interest. As an inhomogeneous pattern in w develops from the homogeneous state, we study interactions between the components of $\mathbf{v}$ when all are of order ε:

$$|v_i(x)| \ll 1, \forall i = 1,\ldots,6, \quad \forall x \in X. \tag{43}$$

Each cortical-map "feature" $v_i(x)$ is a linear functional of $w(x,r)$, hence of $h(x,r) = (w(x,r) - w_0(x,r))/\varepsilon$ corresponding to a component of one of the zeroth, first or second vector moments of w with respect to r at cortical location x. Therefore the dynamical behavior of each is described by the corresponding moment of Eq. 12 (see Table 1 for the moment definitions):

$$\frac{d}{dt}\hat{\lambda}(x) = \eta \int_{r\in\mathbb{R}^2} \mathbf{F}[w](x,r)\,dr \tag{44}$$

$$\frac{d}{dt}(\lambda(x)s(x)) = \eta \int_{r\in\mathbb{R}^2} \mathbf{F}[w](x,r)\left(r - \frac{x}{\mu}\right)dr \tag{45}$$

$$\frac{d}{dt}(\lambda(x)\chi(x)) = \eta \int_{u\in\mathbb{R}^2} \mathbf{F}[w](x,u+R(x))\begin{pmatrix} u_1^2 - u_2^2 \\ 2u_1u_2\end{pmatrix}du \tag{46}$$

$$\frac{d}{dt}(\lambda(x)\rho(x)) = \eta \int_{u\in\mathbb{R}^2} \mathbf{F}[w](x,u+R(x))\frac{||u||^2}{2}\,du \tag{47}$$

Recall that the retinotopy $R(x) = s(x) + x/\mu$ includes the order ε retinotopic distortion.

There is a cascade of perturbation effects from lower moments to higher moments. Inhomogeneities in $\lambda(x)$ affect all the higher moments, as evident in Eqs. 44–47. Inhomogeneities in the retinotopy vector $s(x)$ affect the dynamics of the orientation vector and the receptive field width.

The dynamical constraints on weight evolution (Eq. 12) include a logistic constraint on the net fan-out weight $\Upsilon(r)$ from each geniculate location r. In the homogeneous state the fan-out has a uniform value $\Upsilon_0 = \mu^2\lambda_0$, where μ is the geniculocortical

magnification factor. Variation of the fan-in weight, the centers of the receptive fields or their elongation in various directions spoil the uniformity of the fan-out, inducing a perturbation $\hat{\Upsilon}(r) = \Upsilon(r) - \Upsilon_0$. In this way the logistic Υ-term provides reinforcement of the homogeneous state.

Two matrices that arise frequently in calculations with the orientation vector are $S_1 = \begin{pmatrix} 1 & \\ & -1 \end{pmatrix}$ and $S_2 = \begin{pmatrix} & 1 \\ 1 & \end{pmatrix}$. Thus $u^T S_1 u$ and $u^T S_2 u$ are shorthand for $u_1^2 - u_2^2$ and $2u_1u_2$, respectively.

To first order in $\hat{\lambda}/\lambda_0$, s, χ and ρ, a perturbed receptive field profile for cortical location x is given by:

$$\begin{aligned} w(x,r) &= (\lambda_0 + \hat{\lambda}(x)) \cdot g\left(r - \frac{x}{\mu} - s(x), (\sigma_0^2 + \rho(x))I_2 + \frac{1}{2}\begin{pmatrix} \chi_1(x) & \chi_2(x) \\ \chi_2(x) & -\chi_1(x) \end{pmatrix}\right) \\ &= \lambda_0 g\left(r - \frac{x}{\mu}, \sigma_0^2\right) \cdot \left\{ 1 + \frac{\hat{\lambda}(x)}{\lambda_0} \right. \\ &\quad + \frac{(r - x/\mu) \cdot s(x)}{\sigma_0^2} + \frac{\rho(x)}{\sigma_0^2}\left(\frac{||r - x/\mu||^2}{2\sigma_0^2} - 1\right) \\ &\quad \left. + \frac{1}{4\sigma_0^4}(\chi_1(x)(r-x/\mu)^T S_1 (r-x/\mu) + \chi_2(x)(r-x/\mu)^T S_2 (r - x/\mu)) \right\} \\ &\quad + O((\hat{\lambda}, s, \chi, \rho)^2) \end{aligned} \tag{48}$$

The fan-out for the perturbed weights is calculated to first order below, see Eq. 56. Substituting the first-order perturbed weights 48 and 56 into the dynamical systems Eq. 12 and calculating the moments as in Eq. 44 yields equations for the interactions mediated by the direct "geometrical" effects of lower moments on higher. For Gaussian identities used in calculating the moment integrals see Table 8 in Appendix A. We are now in a position to derive the evolution of the moments:

$$\frac{1}{\eta}\frac{d}{dt}\frac{\hat{\lambda}(x)}{\lambda_0} = \lambda A * \left(\frac{\hat{\lambda}}{\lambda_0}\right) - \alpha\left(\frac{\hat{\lambda}}{\lambda_0}\right) - c_\lambda \hat{\lambda} - c_\Upsilon \int_u \hat{\Upsilon}(u + R(x)) g(u, \sigma_0^2)\, du \tag{49}$$

$$\frac{1}{\eta}\frac{d}{dt}s(x) = \lambda A * s - \alpha s - \lambda\left(A\frac{x}{\mu}\right) * \left(\frac{\hat{\lambda}}{\lambda_0}\right) - c_\Upsilon \int_u \hat{\Upsilon}(u + R(x)) g(u, \sigma_0^2) u\, du \tag{50}$$

$$\begin{aligned} \frac{1}{\eta}\frac{d}{dt}\chi_1(x) &= \lambda A * \chi_1 - \alpha\chi_1 + \lambda\left(A\frac{x^T S_1 x}{\mu^2}\right) * \left(\frac{\hat{\lambda}}{\lambda_0}\right) + 2\lambda\left(A\frac{x^T}{\mu}\right) * (S_1 s) \\ &\quad - c_\Upsilon \int_u \hat{\Upsilon}(u + R(x)) g(u, \sigma_0^2)(u^T S_1 u)\, du \end{aligned} \tag{51}$$

$$\frac{1}{\eta}\frac{d}{dt}\chi_2(x) = \lambda A * \chi_2 - \alpha\chi_2 + \lambda\left(A\frac{x^T S_2 x}{\mu^2}\right) * \left(\frac{\hat{\lambda}}{\lambda_0}\right) + 2\lambda\left(A\frac{x^T}{\mu}\right) * (S_2 s)$$
$$-c_\gamma \int_u \hat{\gamma}(u + R(x)) g(u, \sigma_0^2)(u^T S_2 u)\, du \tag{52}$$

$$\frac{1}{\eta}\frac{d}{dt}\rho(x) = \lambda A * \rho - \alpha\rho + \left(A\left(\lambda\frac{||x||^2}{\mu^2} + \sigma_r^2\right)\right) * \left(\frac{\hat{\lambda}}{\lambda_0}\right) + 2\lambda\left(A\frac{x^T}{\mu}\right) * s$$
$$-c_\gamma \int_u \hat{\gamma}(u + R(x)) g(u, \sigma_0^2)(||u||^2 - \sigma_0^2)\, du \tag{53}$$

Each quantity $\dot{v}_i/\eta$ has a term $\lambda A * v_i - \alpha v_i$ pitting Turing-type pattern growth due to the difference-of-Gaussians lateral interaction A against the decay rate α. Here $*$ denotes convolution in the x variable:

$$((f) * (g))(x) := \int_{x' \in \mathbb{R}^2} f(x - x') g(x')\, dx'.$$

Therefore each component of the vector separately obeys dynamics that can form patterns when λ increases beyond a critical value—although this value may be different for different components v_i. Because each of these self-interaction terms arises from the same underlying pattern-forming mechanism $A*$, *each component of the cortical map will become unstable to patterns at a common wavelength.* This common length scale justifies the assumption in Thomas and Cowan (2004) of plane-periodic solutions in all components at once, and simplifies the search for bifurcating solutions considerably.

The logistic fan-in constraint makes the fan-in deviation $\hat{\lambda}(x)$ decay at a rate c_λ. If there is a finite deviation of the net input weight from its uniform equilibrium value λ_0, then each of the other $\dot{v}_i$ is influenced by a convolution term of the form

$$\lambda\left(Af_i'\left(\frac{x}{\mu}\right)\right) * \left(\frac{\hat{\lambda}}{\lambda_0}\right) := \lambda \int_{x' \in \mathbb{R}^2} A(x - x') f_i'\left(\frac{(x - x')}{\mu}\right)\left(\frac{\hat{\lambda}(x)}{\lambda_0}\right) dx'$$

where $f_i'(u)$ generates a vector moment:

$$f_i'(u) = \begin{cases} u_1, & i = 2 \\ u_2, & i = 3 \\ u^T S_1 u, & i = 4 \\ u^T S_2 u, & i = 5 \\ ||u||^2 + \sigma_r^2/\lambda, & i = 6 \end{cases}. \tag{54}$$

The various convolution kernels $A(x) f_i'(x/\mu)$ are pictured in Fig. 4. Also shown is $A(x)$, corresponding to $f_1'(x) := \mathbf{1}$.

Just as deviations in the zeroth moment or fan-in weight affect the evolution of all higher moments, so do deviations in the first moment, $s(x)$, affect the second-order

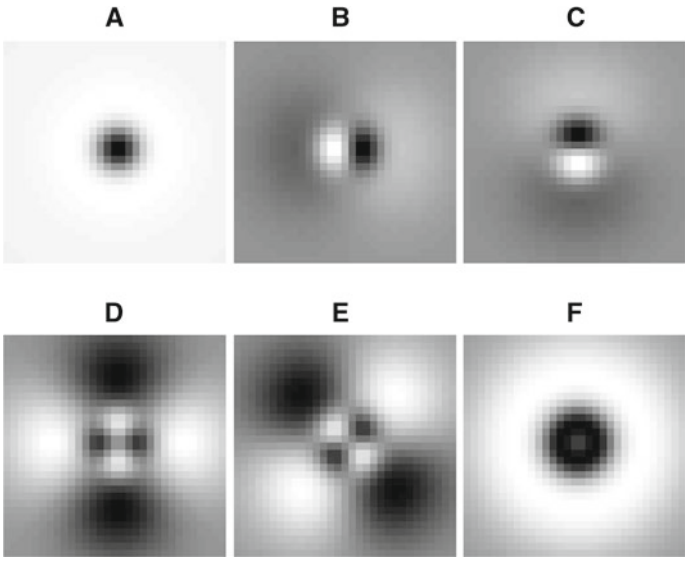

Fig. 4 Convolution kernels for the first-order interactions in Eqs. 49–53 induced by dependence of higher moments on lower moments. **a** $A(x)$. **b** $A(x)\frac{x_1}{\mu}$. **c** $A(x)\frac{x_2}{\mu}$. **d** $A(x)\frac{x^T S_1 x}{\mu^2}$. **e** $A(x)\frac{x^T S_2 x}{\mu^2}$. **f** $A(x)\left(\lambda\frac{||x||^2}{\mu^2}+\sigma_r^2\right)$. *Dark* indicates positive values

moment components $\chi_1(x)$, $\chi_2(x)$ and $\rho(x)$. The fourth terms in Eqs. 51, 52 and 53 combine convolution with an inner product. For example, the fourth term for the $\dot{\rho}$ expression is interpreted as

$$\left(A\frac{x^T}{\mu}\right) * s = \int\limits_{x'\in\mathbb{R}^2} A(x-x')((x_1-x_1')s_1(x')+(x_2-x_2')s_2(x'))\,dx'.$$

The terms for the two χ components are interpreted similarly.

Each expression for $\dot{v}_i$ ends with a term, resulting from the fan-out constraint, of the form

$$-c_\Upsilon \int\limits_u \hat{\Upsilon}(u+R(x))g(u,\sigma_0^2)f_i(u)\,du, \quad f_i(u)=\begin{cases}1, & i=1\\ u_1, & i=2\\ u_2, & i=3\\ u^T S_1 u, & i=4\\ u^T S_2 u, & i=5\\ ||u||^2-\sigma_0^2, & i=6\end{cases}. \quad (55)$$

With the exception of f_6 these functions are identical to the f_i' that arose from the fan-in constraint term.

To obtain the full interactions we eliminate the fan-out terms by rewriting the fan-out explicitly in terms of cortical-map components **v**. The fan-out deviation $\hat{\Upsilon}(r)$ induced by $\hat{\lambda}/\lambda_0$, s, χ and ρ is found by integrating the first-order Taylor expansion of the

perturbed weight profile $w(x, r)$, Eq. 48, in the x variable. Once $\hat{\Upsilon}(r)$ is obtained the integrals in Eq. 55 may be computed, via the Gaussian identities in Table 8 (Appendix A). Substituting these integrals back into Eqs. 49–53 completes the calculation.

To first order in $\hat{\lambda}/\lambda_0, s, \chi$ and ρ the perturbed fan-out is given by:

$$\begin{aligned}\hat{\Upsilon}(r) = &\int_{x'} g(r - x'/\mu, \sigma_0^2)\hat{\lambda}(x')\,dx' \\ &+ \frac{\lambda_0}{\sigma_0^2}\int_{x'} g(r - x'/\mu, \sigma_0^2)(r - x'/\mu)\cdot s(x')\,dx' \\ &+ \frac{\lambda_0}{4\sigma_0^4}\int_{x'} g(r - x'/\mu, \sigma_0^2)(r - x'/\mu)^T S_1(r - x'/\mu)\chi_1(x')\,dx' \\ &+ \frac{\lambda_0}{4\sigma_0^4}\int_{x'} g(r - x'/\mu, \sigma_0^2)(r - x'/\mu)^T S_2(r - x'/\mu)\chi_2(x')\,dx' \\ &+ \frac{\lambda_0}{\sigma_0^2}\int_{x'} g(r - x'/\mu, \sigma_0^2)\left(\frac{||r - x'/\mu||^2}{2\sigma_0^2} - 1\right)\rho(x')\,dx' \\ &+ O((\hat{\lambda}/\lambda_0, s, \chi, \rho)^2). \end{aligned} \tag{56}$$

The integrals arising from the fan-out perturbation terms in Eq. 55 are given in Table 3. For convenience, we adopt the following shorthand:

$$G(x) := g\left(\frac{x}{\mu}, 2\sigma_0^2 I\right)$$

where $g(u, \sigma_0^2 I)$ is the symmetric planar normal distribution with width σ_0 as defined by Eq. (15). Also, given planar vector fields $\mathfrak{a}$, $\mathfrak{b}$ and $\mathfrak{c}$ we will adopt the notation

$$\begin{aligned}\left(\begin{bmatrix}\mathfrak{a}_1\\ \mathfrak{a}_2\end{bmatrix}, \begin{bmatrix}\mathfrak{b}_1\\ \mathfrak{b}_2\end{bmatrix}\right) * \begin{bmatrix}\mathfrak{c}_1\\ \mathfrak{c}_2\end{bmatrix} &= \begin{bmatrix}[\mathfrak{a}_1, \mathfrak{b}_1] * \begin{bmatrix}\mathfrak{c}_1\\ \mathfrak{c}_2\end{bmatrix} \\ [\mathfrak{a}_2, \mathfrak{b}_2] * \begin{bmatrix}\mathfrak{c}_1\\ \mathfrak{c}_2\end{bmatrix}\end{bmatrix} \\ &= \begin{bmatrix}(\mathfrak{a}_1 * \mathfrak{c}_1 + \mathfrak{b}_1 * \mathfrak{c}_2) \\ (\mathfrak{a}_2 * \mathfrak{c}_1 + \mathfrak{b}_2 * \mathfrak{c}_2)\end{bmatrix}\end{aligned} \tag{57}$$

This combination of vectors and convolution appears in the last term for the $\hat{\Upsilon}$-integral of $f(u) = u$, see Table 3.

Combining Table 3 and Eqs. 49–53 gives the full interactions, to first order in $\hat{\lambda}/\lambda_0, s, \chi$ and ρ. The resulting expressions take the form given in Eqs. (31) and (32), i.e.

$$\frac{1}{\eta}\frac{d}{dt}\mathbf{v} = -\alpha\mathbf{v} + \lambda A * \mathbf{v} + \mathbf{K} * \mathbf{v}$$

Table 3 Integrals of fan-out constraint terms

$f(u)$	$\int_u \hat{\Upsilon}(u + R(x)) g(u, \sigma_0^2) f(u)\, du$
1	$\lambda_0 G * \left(\frac{\hat{\lambda}}{\lambda_0}\right) + \frac{\lambda_0}{\sigma_0^2}\left(\frac{x^T}{2\mu} G\right) * s$
	$+ \frac{\lambda_0}{4\sigma_0^4}\left(\left[\frac{x^T S_1 x}{4\mu^2}, \frac{x^T S_2 x}{4\mu^2}\right] G\right) * \chi$
	$+ \frac{\lambda_0}{2\sigma_0^4}\left(\left(\frac{\|x\|^2}{4\mu^2} + \frac{\sigma_0^2}{2}\right) G\right) * \rho$
u	$\lambda_0 \left(\frac{x}{2\mu} G\right) * \left(\frac{\hat{\lambda}}{\lambda_0}\right) + \frac{\lambda_0}{\sigma_0^2}\left(\left(\frac{\sigma_0^2}{2} I_2 - \frac{x x^T}{4\mu^2}\right) G\right) * s$
	$+ \frac{\lambda_0}{4\sigma_0^4}\left(\left[\left(\sigma_0^2 I_2 - \frac{x x^T}{4\mu^2}\right) S_1 \frac{x}{2\mu}, \left(\sigma_0^2 I_2 - \frac{x x^T}{4\mu^2}\right) S_2 \frac{x}{2\mu}\right] G\right) * \chi$
	$+ \frac{\lambda_0}{2\sigma_0^4}\left(\left(2\sigma_0^2 - \frac{\|x\|^2}{4\mu^2}\right) \frac{x}{2\mu} G\right) * \rho$
$u^T S_i u$	$\lambda_0 \left(\frac{x^T S_i x}{4\mu^2} G\right) * \left(\frac{\hat{\lambda}}{\lambda_0}\right) + \frac{\lambda_0}{\sigma_0^2}\left(\left(\frac{x^T S_i x x^T}{8\mu^3} - \sigma_0^2 \frac{x^T}{2\mu} S_i\right) G\right) * s$
$(i = 1, 2)$	$+ \frac{\lambda_0}{4\sigma_0^4}\left\{\left(\left[\frac{x^T S_i x x^T S_1 x}{16\mu^4}, \frac{x^T S_i x x^T S_2 x}{16\mu^4}\right] G\right) * \chi\right.$
	$\left. - \left(\left(2\sigma_0^2 \frac{\|x\|^2}{4\mu^2} - \sigma_0^4\right) G\right) * \chi_i\right\}$
	$+ \frac{\lambda_0}{2\sigma_0^4}\left(\frac{x^T S_i x}{4\mu^2}\left(\frac{\|x\|^2}{4\mu^2} - 3\sigma_0^2\right) G\right) * \rho$
$\|u\|^2$	$\lambda_0 \left(\left(\frac{\|x\|^2}{4\mu^2} + \sigma_0^2\right) G\right) * \left(\frac{\hat{\lambda}}{\lambda_0}\right) + \frac{\lambda_0}{\sigma_0^2}\left(\frac{\|x\|^2 x^T}{8\mu^3} G\right) * s$
	$+ \frac{\lambda_0}{4\sigma_0^4}\left(\left[\frac{x^T S_1 x}{4\mu^2}, \frac{x^T S_2 x}{4\mu^2}\right]\left(\frac{\|x\|^2}{4\mu^2} - \sigma_0^2\right) G\right) * \chi$
	$+ \frac{\lambda_0}{2\sigma_0^4}\left(\left(\frac{\|x\|^2}{4\mu^2} - 2\sigma_0^2\right) G \frac{\|x\|^2}{4\mu^2}\right) * \rho$

The vector convolution notation is defined in Eq. (57)

Table 4 First-order influence of fan-in on cortical-map vector, given by K_{ij} for $i = 1$ to 6 and $j = 1$

K_{ij}	$j = 1$
$i = 1$	$-\lambda_0 (c_\Upsilon G + c_\lambda \delta)$
$\binom{i = 2}{i = 3}$	$-\lambda\left(\frac{x}{\mu} A\right) - \lambda_0 c_\Upsilon \left(\frac{x}{2\mu} G\right)$
$i = 4$	$\lambda \frac{x^T S_1 x}{\mu^2} A - \lambda_0 c_\Upsilon \frac{x^T S_1 x}{4\mu^2} G$
$i = 5$	$\lambda \frac{x^T S_2 x}{\mu^2} A - \lambda_0 c_\Upsilon \frac{x^T S_2 x}{4\mu^2} G$
$i = 6$	$\left(\lambda \frac{\|x\|^2}{\mu^2} + \sigma_r^2\right) A - \lambda_0 c_\Upsilon \frac{\|x\|^2}{4\mu^2} G$

where $\mathbf{K}$ is a six-by-six matrix of convolution kernels and

$$(\mathbf{K} * \mathbf{v})_i := \sum_{j=1}^{6} \left(\int_{x' \in \mathbb{R}^2} \mathbf{K}_{ij}(x - x') \mathbf{v}_j(x')\, dx' \right).$$

The convolution kernels composing $\mathbf{K}$ are given in Tables 4, 5, 6 and 7. Each convolution kernel K_{ij} gives the first-order influence of the jth component of the cortical-map

Table 5 First-order influence of retinotopic distortion on cortical-map vector, given by K_{ij} for $i = 1$ to 6 and $j = 2, 3$

K_{ij}	$(j = 2, j = 3)$
$i = 1$	$-c_\Upsilon \frac{\lambda_0}{\sigma_0^2}\left(\frac{x^T}{2\mu} G\right)$
$\begin{pmatrix} i = 2 \\ i = 3 \end{pmatrix}$	$-c_\Upsilon \frac{\lambda_0}{\sigma_0^2}\left(\left(\frac{\sigma_0^2}{2} I_2 - \frac{xx^T}{4\mu^2}\right) G\right)$
$i = 4$	$2\lambda \frac{x^T}{\mu} A S_1 - \frac{\lambda_0 c_\Upsilon}{\sigma_0^2} \frac{x^T}{2\mu} S_1 \left(\frac{xx^T}{4\mu^2} - \sigma_0^2 I_2\right) G$
$i = 5$	$2\lambda \frac{x^T}{\mu} A S_2 - \frac{\lambda_0 c_\Upsilon}{\sigma_0^2} \frac{x^T}{2\mu} S_2 \left(\frac{xx^T}{4\mu^2} - \sigma_0^2 I_2\right) G$
$i = 6$	$2\lambda \frac{x^T}{\mu} A - \frac{\lambda_0 c_\Upsilon}{\sigma_0^2}\left(\frac{\|x\|^2}{4\mu^2} - \sigma_0^2\right) \frac{x^T}{2\mu} G$

Table 6 First-order influence of orientation components on cortical-map vector, given by K_{ij} for $i = 1$ to 6 and $j = 4, 5$

K_{ij}	$j = 4$	$j = 5$
$i = 1$	$-c_\Upsilon \frac{\lambda_0}{4\sigma_0^4} \frac{x^T S_1 x}{4\mu^2} G$	$-c_\Upsilon \frac{\lambda_0}{4\sigma_0^4} \frac{x^T S_2 x}{4\mu^2} G$
$\begin{pmatrix} i = 2 \\ i = 3 \end{pmatrix}$	$-c_\Upsilon \frac{\lambda_0}{4\sigma_0^4}\left(\left(\sigma_0^2 - \frac{xx^T}{4\mu^2}\right) S_1 \frac{x}{2\mu} G\right)$	$-c_\Upsilon \frac{\lambda_0}{4\sigma_0^4}\left(\left(\sigma_0^2 - \frac{xx^T}{4\mu^2}\right) S_2 \frac{x}{2\mu} G\right)$
$i = 4$	$-c_\Upsilon \frac{\lambda_0}{4\sigma_0^4}\left(\frac{(x^T S_1 x)^2}{16\mu^4} - 2\sigma_0^2 \frac{\|x\|^2}{4\mu^2} + \sigma_0^4\right) G$	$-c_\Upsilon \frac{\lambda_0}{4\sigma_0^4} \frac{x^T S_1 x x^T S_2 x}{16\mu^4} G$
$i = 5$	$-c_\Upsilon \frac{\lambda_0}{4\sigma_0^4} \frac{x^T S_1 x x^T S_2 x}{16\mu^4} G$	$-c_\Upsilon \frac{\lambda_0}{4\sigma_0^4}\left(\frac{(x^T S_2 x)^2}{16\mu^4} - 2\sigma_0^2 \frac{\|x\|^2}{4\mu^2} + \sigma_0^4\right) G$
$i = 6$	$-c_\Upsilon \frac{\lambda_0}{4\sigma_0^4} \frac{x^T S_1 x}{4\mu^2}\left(\frac{\|x\|^2}{4\mu^2} - 2\sigma_0^2\right) G$	$-c_\Upsilon \frac{\lambda_0}{4\sigma_0^4} \frac{x^T S_2 x}{4\mu^2}\left(\frac{\|x\|^2}{4\mu^2} - 2\sigma_0^2\right) G$

Table 7 First-order influence of receptive-field width on cortical-map vector, given by K_{ij} for $i = 1$ to 6 and $j = 6$

K_{ij}	$j = 6$
$i = 1$	$-c_\Upsilon \frac{\lambda_0}{2\sigma_0^4}\left(\left(\frac{\|x\|^2}{4\mu^2} + \frac{\sigma_0^2}{2}\right) G\right)$
$\begin{pmatrix} i = 2 \\ i = 3 \end{pmatrix}$	$-c_\Upsilon \frac{\lambda_0}{2\sigma_0^4}\left(\left(2\sigma_0^2 - \frac{\|x\|^2}{4\mu^2}\right) \frac{x}{2\mu} G\right)$
$i = 4$	$-c_\Upsilon \frac{\lambda_0}{2\sigma_0^4}\left(\frac{x^T S_1 x}{4\mu^2}\left(\frac{\|x\|^2}{4\mu^2} - 3\sigma_0^2\right) G\right)$
$i = 5$	$-c_\Upsilon \frac{\lambda_0}{2\sigma_0^4}\left(\frac{x^T S_2 x}{4\mu^2}\left(\frac{\|x\|^2}{4\mu^2} - 3\sigma_0^2\right) G\right)$
$i = 6$	$-c_\Upsilon \frac{\lambda_0}{2\sigma_0^4}\left(\frac{\|x\|^4}{16\mu^4} - 3\sigma_0^2 \frac{\|x\|^2}{4\mu^2} - \frac{\sigma_0^4}{2}\right) G$

vector $v_j(x)$ on the development of the ith component $v_i(x)$. The influence of the two retinotopic-distortion components on the two-vector representing the orientation map, for example, is given by the four convolution kernels

$$\begin{pmatrix} K_{42} & K_{43} \\ K_{52} & K_{53} \end{pmatrix}$$

in Table 6. Each component also interacts with itself through convolution with the difference-of-Gaussians λA, as well as obeying intrinsic decay at rate α.

Table 8 Identities for integrals of the form $\int_{u\in\mathbb{R}^2} f(u)g(u+v,\sigma^2/2)\,du$, where $g(u,\sigma^2) := \exp\left(-||u||^2/\left(2\sigma^2\right)\right)/\left(2\pi\sigma^2\right)$, for various functions $f(u)$. Note $u=(u_1,u_2)^T\in\mathbb{R}^2$

$f(u)$	$\int_{u\in\mathbb{R}^2} f(u)g(u+v,\sigma^2/2)\,du$
1	1
u_j	$-v_j$
u_1u_2	v_1v_2
u_i^2	$v_i^2+\sigma^2/2$
$\|\|u\|\|^2$	$\|\|v\|\|^2+\sigma^2$
u_j^3	$-v_j(v_j^2+3\sigma^2/2)$
$u_i^2u_j, i\neq j$	$-(v_i^2+\sigma^2/2)v_j$
u_i^4	$v_i^4+3\sigma^2v_i^2+3\sigma^4/4$
$u_i^3u_j, i\neq j$	$v_iv_j(v_1^2+3\sigma^2/2)$
$u_1^2u_2^2$	$v_1^2v_2^2+\|\|v\|\|^2\sigma^2/2+\sigma^4/4$
$\|\|u\|\|^4$	$\|\|v\|\|^4+4\sigma^2\|\|v\|\|^2+2\sigma^4$

5 Discussion

The example given in Sect. 4.3 shows the extreme case of reduction of a full synaptic model to a model for the development of a single feature map, $\phi(x)$. We may instead choose to let both $\phi(x)$ and $q(x)$ vary, in which case the update rule specifies a change in the vector $\chi(x)=q(x)(\cos 2\phi(x),\sin 2\phi(x))^T$:

$$\Delta\chi(x)=\eta\int_{x'}A(x-x')\chi(x')\,dx'. \tag{58}$$

Allowing all the components to vary at once leads to coupling between higher and lower moments that to linear order (small deviations from the uniform, isotropic state) takes the form of Eq. (31). A similar method may be used to study ocular dominance.[5] Starting from a pair of $w_1(x,r)$, $w_2(x,r)$ representing feedforward synaptic weight distributions from two different input layers labeled with a common set of retinotopic coordinates, one for each eye, leads to a spatially extended Ising model. In this case we define net fan-in weights $\lambda_j(x)=\int_r w_j(x,r)\,dr$ for each input layer ($j=1,2$) and define the ocular dominance $z(x)$ as the normalized weight difference $z(x)=(\lambda_1(x)-\lambda_2(x))/(\lambda_1(x)+\lambda_2(x))$. Derivation of the spatially extended Ising model proceeds as above, with the additional requirement that one specify both a same-eye correlation function $C_{ii}(r-r')$ and a cross-eye correlation $C_{ij}(r-r'), i\neq j$.

[5] Related models for spontaneous formation of ocular dominance patterns through constrained Hebbian mechanisms have been discussed in Bressloff (2005); Bressloff and Oster (2010); Harris et al. (1997, 2000); Osan and Ermentrout (2002); Oster and Bressloff (2006).

In each case, Euclidean symmetry of the linear system and the steady state leads to degeneracy of the eigenvalues at a symmetry-breaking bifurcation. The analysis of solutions of the pattern-formation problem depends on the techniques of equivariant bifurcation theory, similar to those used to analyze pattern formation underlying the analysis of geometric visual hallucinations (Bressloff et al. 2001a,b, 2002; Ermentrout and Cowan 1979). In this framework, when the uniform steady state loses stability, the equivariant branching lemma (Golubitsky et al. 1988) guarantees the existence of solutions or planforms with particular symmetries [the symmetry of the so called *axial subgroups* (Golubitsky and Stewart 2004)]. In order to guarantee the existence of such solutions, one typically restricts attention to spatially periodic solutions on one of the planar lattices. On the other hand, Wolf has shown that relaxing the restriction to lattice periodic solutions allows one to consider larger families of planforms, obtained from superposition of large numbers of individual plane wave solutions (Wolf 2005). The resulting orientation map patterns show remarkable correspondence to features of visual cortex across species, such as the density of orientation singularities (pinwheels) relative to the typical orientation map periodicity length (Kaschube et al. 2010). To our knowledge, the corresponding superposition of multiple plane waves has not been studied in the multidimensional map context (orientation, retinotopy, net input, and receptive field width), but only subject to the lattice periodic restriction (Thomas and Cowan 2004).

The model described here has several advantages when compared with similar models previously developed. The use of soft constraints on the net fan-in and fan-out weights instead of hard nonlinearities allows us to study the developmental pattern-formation process analytically. By avoiding the use of arbor functions (Miller 1994), which provide a priori constraints on the retinotopic structure of the weight distribution, our method permits us to study the formation of fine-grain structure in the retinotopic map as well as the orientation map simultaneously. By starting from a high-dimensional representation we naturally arrive at developmental rules in which low-dimensional features such as orientation and retinotopy are coupled together. In particular, the model has been shown to predict a positive correlation between dislocations in the orientation map and in the local retinotopic map (Thomas and Cowan 2004), consistent with some experimental findings (Das and Gilbert 1997).

The synaptic weights develop on a slow timescale compared to the relaxation time of the output-layer activity. Here we used a learning rule based solely on the mean correlation of input-layer and output-layer activities, i.e. a rate-based rather than timing-based rule. The derivation of low-dimensional map development rules may be extended to include velocity-tuning (Yao et al. 2007) or looming (Wicklein and Strausfeld 2000) in addition to orientation, for example, by using a timing-based learning rule. Extension of the method described here to a more realistic simple cell receptive field structure with positive and negative subfields is plausible, but has not yet been attempted. Alternatively, the synaptic weight model considered here could be viewed as the mean field version of a finer grained model. Recent innovations in the treatment of statistical neural field models beyond the mean field (Buice and Cowan

2007, 2009; Buice et al. 2010) could suggest additional directions for expanding this work.

Acknowledgements PJT acknowledges the support of the National Science Foundation (grants DMS-0720142, DMS-1010434 and EF-1038677) and the Oberlin College Libraries.

Appendix A: Gaussian identities

Let $u = \begin{pmatrix} u_1 \\ u_2 \end{pmatrix}$ and $v = \begin{pmatrix} v_1 \\ v_2 \end{pmatrix}$ denote vectors in the plane, and let σ be a positive real number. Define $g(u, \sigma^2) := \exp(-||u||^2/(2\sigma^2))/(2\pi\sigma^2)$. Then the following identities hold:

$$\int_{\mathbb{R}^2} g(u, \sigma^2)\, du = 1 \tag{59}$$

$$\int_{\mathbb{R}^2} u g(u - v, \sigma^2)\, du = v \tag{60}$$

$$\int_{\mathbb{R}^2} |u|^2 g(u, \sigma^2)\, du = \sigma^2 \tag{61}$$

$$\int_{\mathbb{R}^2} g(u - v, \sigma_u^2) g(v, \sigma_v^2)\, dv = g(u, \sigma_u^2 + \sigma_v^2) \tag{62}$$

$$g(u, \sigma_1^2) g(u, \sigma_2^2) = \frac{g(u, \sigma_1^2 \sigma_2^2/(\sigma_1^2 + \sigma_2^2))}{2\pi(\sigma_1^2 + \sigma_2^2)} \tag{63}$$

$$g(u - v, \sigma^2) g(u' - v, \sigma^2) = g(u - u', (2\sigma)^2) g\left(\frac{u + u'}{2} - v, \left(\frac{\sigma}{2}\right)^2\right) \tag{64}$$

Let two quadratic forms (see Appendix B) P and Q be given by

$$P = \frac{\mathrm{Tr} P}{2} I_2 + \frac{q[P]}{2} \Phi_2(\phi[P])$$
$$Q = \frac{\mathrm{Tr} Q}{2} I_2 + \frac{q[Q]}{2} \Phi_2(\phi[Q]).$$

In analogy with the notation $g(u, \sigma^2)$ given above, define

$$g(u, Q) = \frac{1}{2\pi\sqrt{\det Q}} \exp\left(-\frac{1}{2} u^T Q^{-1} u\right) \tag{65}$$

Then the convolution of two such Gaussians is again a Gaussian

$$\int_{u\in\mathbb{R}^2} g(u-u',P)g(u',Q)\,du' = g(u,C) \tag{66}$$

where $\mathrm{Tr}C = \mathrm{Tr}P + \mathrm{Tr}Q$. Also, if we write in vector form

$$\begin{aligned}\chi[P] &= q[P]\begin{pmatrix}\cos 2\phi[P]\\ \sin 2\phi[P]\end{pmatrix}\\ \chi[Q] &= q[Q]\begin{pmatrix}\cos 2\phi[Q]\\ \sin 2\phi[Q]\end{pmatrix}\\ \chi[C] &= q[C]\begin{pmatrix}\cos 2\phi[C]\\ \sin 2\phi[C]\end{pmatrix},\end{aligned}$$

then

$$\chi[C] = \chi[P] + \chi[Q]. \tag{67}$$

The effect of a shift in the location of the center by order ϵ is given by the Taylor series:

$$g(u+\epsilon v,\sigma^2) = g(u,\sigma^2)\left(1-\epsilon\frac{v\cdot u}{\sigma^2}+\frac{\epsilon^2}{2\sigma^4}v\cdot\left[\begin{pmatrix}u_1^2-\sigma^2 & u_1u_2\\ u_1u_2 & u_2^2-\sigma^2\end{pmatrix}v\right]+O(\epsilon^3)\right). \tag{68}$$

The calculations in Sect. 4.2 require evaluation of integrals of the form $\int_{u\in\mathbb{R}^2} f(u)\, g(u+v,\sigma^2/2)\,du$, for various polynomial functions $f(u)$. Table 8 provides the needed identities.

Appendix B: Quadratic forms

The covariance matrices that characterize the feed-forward receptive fields in the synaptic model, and other matrix quantities arising in the reduction to the feature model, have geometric properties which are captured by the geometry of quadratic forms. For completeness, we briefly review their properties and establish some notation.

B.1 Degenerate quadratic forms

Given a pair of vectors u, v, take their outer product uv^T to be the matrix $(uv^T)_{ij} = u_iv_j$. The outer product of a planar vector $u = \begin{pmatrix}u_1\\ u_2\end{pmatrix} = |u|\begin{pmatrix}\cos\theta\\ \sin\theta\end{pmatrix}$ with itself is

thus the symmetric matrix

$$uu^T = \begin{pmatrix} u_1^2 & u_1u_2 \\ u_1u_2 & u_2^2 \end{pmatrix} \tag{69}$$

$$= \frac{1}{2}\begin{pmatrix} u_1^2+u_2^2 & \\ & u_1^2+u_2^2 \end{pmatrix} + \frac{|u|^2}{2}\begin{pmatrix} \frac{u_1^2-u_2^2}{|u|^2} & \frac{2u_1u_2}{|u|^2} \\ \frac{2u_1u_2}{|u|^2} & -\frac{(u_1^2-u_2^2)}{|u|^2} \end{pmatrix} \tag{70}$$

$$= \frac{|u|^2}{2}\left\{ I_2 + \begin{pmatrix} \cos^2\theta - \sin^2\theta & 2\cos\theta\sin\theta \\ 2\cos\theta\sin\theta & -(\cos^2\theta - \sin^2\theta) \end{pmatrix}\right\} \tag{71}$$

$$= \frac{|u|^2}{2}\{I_2 + \Phi_2(\theta)\}, \tag{72}$$

where we define

$$\Phi_2(\theta) := \begin{pmatrix} \cos 2\theta & \sin 2\theta \\ \sin 2\theta & -\cos 2\theta \end{pmatrix}. \tag{73}$$

Thus we split uu^T into a multiple of the identity and a traceless part; any traceless 2×2 symmetric matrix A can be written $(\det A)\Phi_2(\theta)$ for some θ. In this case $\theta = \arctan(u_2/u_1)$, which is the angle in the plane made by the vector u (up to $\pm\pi$). The quadratic form uu^T is *degenerate* because the matrix is singular.

B.2 Nondegenerate quadratic forms

Suppose $A = \begin{pmatrix} a & b \\ b & c \end{pmatrix}$ is a covariance matrix with $a > c > 0$ and $\det A > 0$. Then the ellipse given by $u^T Au = r^2$ has its major axis oriented along the direction $\tan 2\phi = \frac{2b}{a-c}$, and its minor axis along $\phi + \frac{\pi}{2}$; its area is proportional to the product of the eigenvalues of A: area $= \pi r^2 \lambda_1\lambda_2 = \pi r^2 \det A$; and its eccentricity is given by $e = \sqrt{1 - \left(\frac{\lambda_2}{\lambda_1}\right)}$.

These standard results may be obtained by decomposing A into a product of two rotations and an anisotropic expansion. Writing α^2 for the ratio of the larger eigenvalue to the smaller, $\alpha := \sqrt{\lambda_1/\lambda_2}$, gives:

$$A = (\det A)^{\frac{1}{2}}\mathrm{Rot}_\phi \Lambda \mathrm{Rot}_{-\phi} \tag{74}$$

$$= \sqrt{\lambda_1\lambda_2}\begin{pmatrix} \cos\phi & -\sin\phi \\ \sin\phi & \cos\phi \end{pmatrix}\begin{pmatrix} \alpha & \\ & \frac{1}{\alpha} \end{pmatrix}\begin{pmatrix} \cos\phi & \sin\phi \\ -\sin\phi & \cos\phi \end{pmatrix} \tag{75}$$

$$= \sqrt{\lambda_1\lambda_2}\begin{pmatrix} \alpha\cos^2\phi + \frac{1}{\alpha}\sin^2\phi & \left(\alpha - \frac{1}{\alpha}\right)\sin\phi\cos\phi \\ \left(\alpha - \frac{1}{\alpha}\right)\sin\phi\cos\phi & \frac{1}{\alpha}\cos^2\phi + \alpha\sin^2\phi \end{pmatrix} \tag{76}$$

$$= \sqrt{\lambda_1\lambda_2}\left(\alpha I_2 + \left(\alpha - \frac{1}{\alpha}\right)\begin{pmatrix} -\sin^2\phi & \sin\phi\cos\phi \\ \sin\phi\cos\phi & -\cos^2\phi \end{pmatrix}\right) \tag{77}$$

$$= \frac{\sqrt{\lambda_1 \lambda_2}}{2} \left(\left(\alpha + \frac{1}{\alpha} \right) I_2 + \left(\alpha - \frac{1}{\alpha} \right) \Phi_2(\phi) \right) \tag{78}$$

where Φ_2 is given by Eq. 73.

We now cast α in terms of $\det A$ and $\mathrm{Tr}A$. The eigenvalues are given by

$$\lambda_{1,2} = \frac{1}{2}\{\mathrm{Tr}A \pm \sqrt{(\mathrm{Tr}A)^2 - 4 \det A}\},$$

from which

$$\alpha = \sqrt{\frac{\lambda_1}{\lambda_2}} = \frac{\mathrm{Tr}A + \sqrt{(\mathrm{Tr}A)^2 - 4 \det A}}{2\sqrt{\det A}}$$
$$\frac{1}{\alpha} = \frac{\mathrm{Tr}A - \sqrt{(\mathrm{Tr}A)^2 - 4 \det A}}{2\sqrt{\det A}}.$$

Hence

$$\alpha + \frac{1}{\alpha} = \frac{\mathrm{Tr}A}{\sqrt{\det A}} \tag{79}$$
$$\alpha - \frac{1}{\alpha} = \frac{\sqrt{(\mathrm{Tr}A)^2 - 4 \det A}}{\sqrt{\det A}}. \tag{80}$$

Thus we have decomposed A into trace and traceless parts given by:

$$A = \frac{\sqrt{\lambda_1 \lambda_2}}{2} \left(\left(\alpha + \frac{1}{\alpha} \right) I_2 + \left(\alpha - \frac{1}{\alpha} \right) \Phi_2(\phi) \right) \tag{81}$$
$$= \frac{\sqrt{\det A}}{2} \left(\frac{\mathrm{Tr}A}{\sqrt{\det A}} I_2 + \frac{\sqrt{(\mathrm{Tr}A)^2 - 4 \det A}}{\sqrt{\det A}} \Phi_2(\phi) \right) \tag{82}$$
$$= \frac{\mathrm{Tr}A}{2} I_2 + \frac{\sqrt{(\mathrm{Tr}A)^2 - 4 \det A}}{2} \Phi_2(\phi) \tag{83}$$
$$= \frac{a+c}{2} I_2 + \frac{\sqrt{(a-c)^2 + 4b^2}}{2} \Phi_2(\phi) \tag{84}$$
$$= \frac{a+c}{2} I_2 + \sqrt{\left(\frac{a-c}{2} \right)^2 + b^2} \begin{pmatrix} \frac{(a-c)/2}{\sqrt{(a-c)^2/4+b^2}} & \frac{b}{\sqrt{(a-c)^2/4+b^2}} \\ \frac{b}{\sqrt{(a-c)^2/4+b^2}} & -\frac{(a-c)/2}{\sqrt{(a-c)^2/4+b^2}} \end{pmatrix} \tag{85}$$
$$= \frac{a+c}{2} I_2 + \begin{pmatrix} \frac{a-c}{2} & b \\ b & -\frac{a-c}{2} \end{pmatrix}; \tag{86}$$

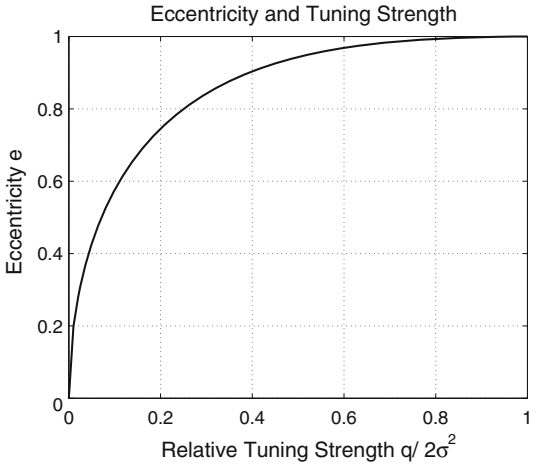

Fig. 5 Eccentricity and magnitude of orientation preference. The *relative* orientation-tuning strength refers to the ratio $q[Q^{-1}]/\mathrm{Tr}Q^{-1}$, which lies between 0 and 1

We can now identify the angle ϕ in the original decomposition as satisfying

$$\cos 2\phi = \frac{a-c}{\sqrt{(a-c)^2+(2b)^2}} \tag{87}$$

$$\sin 2\phi = \frac{2b}{\sqrt{(a-c)^2+(2b)^2}}. \tag{88}$$

This is the angle in the direction of the major axis in the plane of the ellipses associated with the quadratic form A. As a linear transformation, A takes the unit ball in $\mathbf{R^2}$ to an ellipse with area $2\pi \det A$. And the eccentricity is given by the deviation from unity of the ratio of the major and minor axes of the ellipse:

$$e = \sqrt{1-\left(\frac{\lambda_2}{\lambda_1}\right)} = \sqrt{1-\left(\frac{1}{\alpha}\right)^4}.$$

In the treatment in Sect. 4.2, the quantity $q[A] = \sqrt{\mathrm{Tr}^2 A - 4\det A}$ represents the magnitude of the orientation-tuning vector χ. For A a multiple of the identity matrix, $\mathrm{Tr}^2 A = 4\det A$ so $q[A] = 0$. As $\det A$ approaches zero from above, $q[A]$ approaches $\to \mathrm{Tr}A$. Clearly, $0 \le q[A] \le \mathrm{Tr}A$. The eccentricity e may be related to the relative orientation-tuning strength, $q[A]/\mathrm{Tr}A$, as shown in Fig. 5. It may also be represented as the ratio between the geometric and arithmetic means of the pair $(q[A], \mathrm{Tr}A)$:

$$e = \frac{2\sqrt{\mathrm{Tr}A/q[A]}}{1+\mathrm{Tr}A/q[A]} = \frac{\sqrt{q[A]\mathrm{Tr}A}}{(q[A]+\mathrm{Tr}A)/2}.$$

In considering the geometry of receptive fields we deal both with the covariance matrix Q and its inverse Q^{-1}, so we need to know how the two relate as quadratic

forms. Let us rewrite A in terms of its trace, its orientation $\phi[A]$ and its "orientation magnitude" $q[A]$:

$$A = \frac{\mathrm{Tr}A}{2} I_2 + \frac{q[A]}{2} \Phi_2(\phi[A])$$

Since $\Phi_2(\phi)^2 = I_2$ we see at once that

$$\left(\frac{\mathrm{Tr}A}{2} I_2 + \frac{q[A]}{2} \Phi_2(\phi[A])\right)\left(\frac{\mathrm{Tr}A}{2} I_2 - \frac{q[A]}{2} \Phi_2(\phi[A])\right) = \frac{1}{4}((\mathrm{Tr}A)^2 - q[A]^2) I_2$$
$$= \det A \, I_2,$$

whence

$$A^{-1} = \frac{1}{\det A}\left(\frac{\mathrm{Tr}A}{2} I_2 - \frac{q[A]}{2} \Phi_2(\phi[A])\right).$$

Because $A^{-1} = \frac{1}{\det A}\begin{pmatrix} c & -b \\ -b & a \end{pmatrix}$, $\mathrm{Tr}A^{-1} = \frac{\mathrm{Tr}A}{\det A}$. Also, $\Phi_2(\phi - \frac{\pi}{2}) = -\Phi_2(\phi)$, so we can write

$$A^{-1} = \frac{\mathrm{Tr}A^{-1}}{2} I_2 + \frac{q[A^{-1}]}{2} \Phi_2(\phi[A'])$$

where

$$\phi[A^{-1}] = \phi[A] + \frac{\pi}{2}$$
$$q[A^{-1}] = \frac{q[A]}{\det A}.$$

Hence the level curve formed by $u^T A^{-1} u = r^2$ forms an ellipse with major axis oriented orthogonal to that formed by A. Finally, because the eccentricity depends only on the ratio $(\mathrm{Tr}A)^2/\det A$ and because

$$\frac{(\mathrm{Tr}A)^2}{\det A} = \frac{(\mathrm{Tr}A^{-1})^2}{\det A^{-1}},$$

the ellipses formed by A and A^{-1} have the same eccentricity.

References

Bartsch AP, van Hemmen JL (2001) Combined hebbian development of geniculocortical and lateral connectivity in a model of primary visual cortex. Biol Cybern 84(1):41–55

Ben-Yishai R, Sompolinsky H, Bar-Or RL (1995) Theory of orientation tuning in visual cortex. Proc Natl Acad Sci USA 92(9):3844–3848

Binder K, Heermann DW (1997) Solid-State Sciences. In: Monte Carlo simulation in statistical physics: an introduction, vol 80 (3rd edn). Springer Verlag, Heidelberg

Blasdel GG, Salama G (1986) Voltage-sensitive dyes reveal a modular organization in monkey striate cortex. Nature 321(6070):579–585

Blumenfeld B, Bibitchkov D, Tsodyks M (2006) Neural network model of the primary visual cortex: from functional architecture to lateral connectivity and back. J Comput Neurosci 20(2):219–241

Bonhoeffer T, Grinvald A (1991) Orientation columns in cat are organized in pinwheel-like patterns. Nature 353:429–431

Bressloff PC (2005) Spontaneous symmetry breaking in self-organizing neural fields. Biol Cybern 93(4):256–274

Bressloff PC, Oster AM (2010) Theory for the alignment of cortical feature maps during development. Phys Rev E Stat Nonlin Soft Matter Phys 82(2 Pt 1):021920

Bressloff PC, Cowan JD, Golubitsky M, Thomas PJ (2001) Scalar and pseudoscalar bifurcations motivated by pattern formation on the visual cortex. Nonlinearity 14:739–775

Bressloff PC, Cowan JD, Golubitsky M, Thomas PJ, Wiener MC (2001) Geometric visual hallucinations, Euclidean symmetry, and the functional architecture of visual cortex. Philos Trans R Soc Lond B 356:299–330

Bressloff PC, Cowan JD, Golubitsky M, Thomas PJ, Wiener MC (2002) What geometric visual hallucinations tell us about the visual cortex. Neural Comput 14(3):473–491

Buice MA, Cowan JD (2007) Field-theoretic approach to fluctuation effects in neural networks. Phys Rev E Stat Nonlinear Soft Matter Phys 75(5 Pt 1):051919

Buice MA, Cowan JD (2009) Statistical mechanics of the neocortex. Prog Biophys Mol Biol 99(2–3):53–86

Buice MA, Cowan JD, Chow CC (2010) Systematic fluctuation expansion for neural network activity equations. Neural Comput 22(2):377–426

Cardy J (1996) Scaling and renormalization in statistical physics. In: Cambridge lecture notes in physics, vol 5. Cambridge University Press, Cambridge

Chklovskii DB, Schikorski T, Stevens CF (2002) Wiring optimization in cortical circuits. Neuron 34(3):341–347

Cho MW, Kim S (2004) Understanding visual map formation through vortex dynamics of spin hamiltonian models. Phys Rev Lett 92(1):018101

Cho MW, Kim S (2005) Different ocular dominance map formation influenced by orientation preference columns in visual cortices. Phys Rev Lett 94(6):068701

Cowan JD, Friedman EA (1991) Simple spin models for the development of ocular dominance columns and iso-orientation patches. In: Lippmann R, Moody J, Touretzky D (eds) Advances in neural information processing systems 3. Morgan Kaufmann, San Francisco pp 26–31

Das A, Gilbert CD (1997) Distortions of visuotopic map match orientation singularities in primary visual cortex. Nature 387:594–598

Elliott T, Shadbolt NR (2002) Multiplicative synaptic normalization and a nonlinear hebb rule underlie a neurotrophic model of competitive synaptic plasticity. Neural Comput 14(6):1311–1322

Ermentrout GB, Cowan JD (1979) A mathematical theory of visual hallucination patterns. Biol Cybern 34:137–150

Erwin E, Obermayer K, Schulten K (1992) Self-organizing maps: ordering, convergence properties and energy functions. Biol Cybern 67:47–55

Erwin E, Obermayer K, Schulten K (1992) Self-organizing maps: stationary states, metastability and convergence rate. Biol Cybern 67:35–45

Erwin E, Obermayer K, Schulten K (1995) Models of orientation and ocular dominance columns in the visual cortex: a critical comparison. Neural Comput 7(3):425–468

Giacomantonio CE, Ibbotson MR, Goodhill GJ (2010) The influence of restricted orientation rearing on map structure in primary visual cortex. Neuroimage 52(3):875–883

Glauber RJ (1963) Time-dependent statistics of the Ising model. J Math Phys 4(2):294–307

Golubitsky M, Stewart I (2004) The symmetry perspective: from equilibrium to chaos in phase space and physical space. Birhauser, Basel

Golubitsky M, Stewart I, Schaeffer DG (1988) Singularities and groups in bifurcation theory. In: Applied mathematical sciences, vol II. Springer-Verlag, New York

Goodhill GJ, Bates KR, Montague PR (1997) Influences on the global structure of cortical maps. Proc Biol Sci 264(1382):649–655

Goodhill GJ, Cimponeriu A (2000) Analysis of the elastic net model applied to the formation of ocular dominance and orientation columns. Network 11(2):153–168
Goodhill GJ (2007) Contributions of theoretical modeling to the understanding of neural map development. Neuron 56(2):301–311
Harris AE, Ermentrout GB, Small SL (1997) A model of ocular dominance column development by competition for trophic factor. Proc Natl Acad Sci USA 94(18):9944–9949
Harris AE, Ermentrout GB, Small SL (2000) A model of ocular dominance column development by competition for trophic factor: effects of excess trophic factor with monocular deprivation and effects of antagonist of trophic factor. J Comput Neurosci 8(3):227–250
Hastings WK (1970) Monte Carlo sampling methods using Markov chains and their applications. Biometrika 57(1):97–109
Häussler AF, von der Malsburg C (1983) Development of retinotopic projections: an analytical treatment. J Theor Neurobiol 2:47–73
Hawken MJ, Parker AJ (1987) Spatial properties of neurons in the monkey striate cortex. Proc R Soc Lond B Biol Sci 231(1263):251–288
Hirsch JA, Martinez LM (2006) Circuits that build visual cortical receptive fields. Trends Neurosci 29(1):30–39
Hubel DH, Wiesel TN (1962) Receptive fields, binocular interaction and functional architecture of the cat's visual cortex. J Physiol (Lond) 160:106–154
Hubel DH, Wiesel TN (1974) Sequence regularity and geometry of orientation columns in the monkey striate cortex. J Comp Neurol 158(3):267–293
Husson TR, Mallik AK, Zhang JX, Issa NP (2007) Functional imaging of primary visual cortex using flavoprotein autofluorescence. J Neurosci 27(32):8665–8675
Kaschube M, Schnabel M, Löwel S, Coppola DM, White LE, Wolf F (2010) Universality in the evolution of orientation columns in the visual cortex. Science 330(6007):1113–1116
Kosterlitz JM, Thouless DJ (1978) Progress in low temperature physics. In: Two-dimensional Physics, vol VII B, chapter 5. North-Holland, pp 373–433
Koulakov AA, Chklovskii DB (2001) Orientation preference patterns in mammalian visual cortex: a wire length minimization approach. Neuron 29(2):519–527
Malach R, Amir Y, Harel M, Grinvald A (1993) Relationship between intrinsic connections and functional architecture revealed by optical imaging and *in vivo* targeted biocytin injections in primate striate cortex. Proc Natl Acad Sci USA 90:10469–10473
Maldonado PE, Gray CM (1996) Heterogeneity in local distributions of orientation-selective neurons in the cat primary visual cortex. Vis Neurosci 13:509–516
Martinez LM, Wang Q, Reid RC, Pillai C, Alonso J-M, Sommer FT, Hirsch JA (2005) Receptive field structure varies with layer in the primary visual cortex. Nat Neurosci 8(3):372–379
McLaughlin D, Shapley R, Shelley M (2003) Large-scale modeling of the primary visual cortex: influence of cortical architecture upon neuronal response. J Physiol Paris 97(2–3):237–252
Mermin ND, Wagner H (1966) Absence of ferromagnetism or antiferromagnetism in one- or two-dimensional isotropic heisenberg models. Phys Rev Lett 17(22):1133–1136
Metropolis N, Rosenbluth AW, Rosenbluth MN, Teller AH, Teller E (1953) Equation of state calculations by fast computing machines. J Chem Phys 21(6):1087–1092
Miller KD (1994) A model for the development of simple cell receptive fields and the ordered arrangement of orientation columns through activity-dependent competitions between on- and off-center inputs. J Neurosci 14:409–441
Miller KD, MacKay DJC (1994) The role of constraints in hebbian learning. Neural Comput 6:100–126
Mooser F, Bosking WH, Fitzpatrick D (2004) A morphological basis for orientation tuning in primary visual cortex. Nature Neurosci 7(8):872–879
Ohki K, Chung S, Kara P, Hübener M, Bonhoeffer T, Reid RC (2006) Highly ordered arrangement of single neurons in orientation pinwheels. Nature 442(7105):925–928
Ohki K, Reid RC (2007) Specificity and randomness in the visual cortex. Curr Opin Neurobiol 17(4):401 – 407 (sensory systems)
Ohshiro T, Weliky M (2006) Simple fall-off pattern of correlated neural activity in the developing lateral geniculate nucleus. Nat Neurosci 9(12):1541–1548
Osan R, Ermentrout B (2002) Development of joint ocular dominance and orientation selectivity maps in a correlation-based neural network model. Neurocomputing 44–46(0):561–566
Oster AM, Bressloff PC (2006) A developmental model of ocular dominance column formation on a growing cortex. Bull Math Biol 68(1):73–98

Paik S-B, Ringach D (2010) Orientation maps as Moiré interference of retinal ganglion cell mosaics. In: Conference Abstract: Computational and Systems Neuroscience. Frontiers in Systems Neuroscience
Reggia JA, Montgomery D (1996) A computational model of visual hallucinations in migraine. Comput Biol Med 26(2):133–141
Reid RC, Alonso JM (1995) Specificity of monosynaptic connections from thalamus to visual cortex. Nature 378(6554):281–284
Reyes AD (2010) Input-dependent switching of inhibitory configurations in neural networks. In: Conference Abstract: Computational and Systems Neuroscience. Frontiers in Systems Neuroscience
Ringach DL (2004) Mapping receptive fields in primary visual cortex. J Physiol 558(Pt 3):717–728
Ringach DL (2007) On the origin of the functional architecture of the cortex. PLoS One 2(2):e251
Shoham D, Hübener M, Schulze S, Grinvald A, Bonhoeffer T (1997) Spatio-temporal frequency domains and their relation to cytochrome oxidase staining in cat visual cortex. Nature 385:529–533
Somers DC, Nelson SB, Sur M (1995) An emergent model of orientation selectivity in cat visual cortical simple cells. J Neurosci 15(8):5448–5465
Song S, Miller KD, Abbott LF (2000) Competitive hebbian learning through spike-timing-dependent synaptic plasticity. Nat Neurosci 3(9):919–926
Swindale NV (1991) Coverage and the design of striate cortex. Biol Cybern 65:415–424
Swindale NV (1996) The development of topography in the visual cortex: a review of models. Network 7(2):161–247
Swindale NV, Shoham D, Grinvald A, Bonhoeffer T, Hübener M (2000) Visual cortex maps are optimized for uniform coverage. Nat Neurosci 3(8):822–826
Tanaka S (1990) Theory of self-organization of cortical maps: Mathematical framework. Neural Netw 3:625–640
Thomas PJ (2000) Order and disorder in visual cortex: spontaneous symmetry-breaking and statistical mechanics of pattern formation in vector models of cortical development. Ph.D. Thesis, The University of Chicago, Department of Mathematics, August 2000
Thomas PJ, Cowan JD (2004) Symmetry induced coupling of cortical feature maps. Phys Rev Lett 92(18):e188101
Thomas PJ, Cowan JD (2006) Simultaneous constraints on pre- and post-synaptic cells couple cortical feature maps in a 2d geometric model of orientation preference. Math Med Biol 23(2):119–138 (epub April 20, 2006)
Tootell RBH, Hamilton SL, Silverman MS, Switkes E (1988) Functional anatomy of macaque striate cortex. I. Ocular dominance, binocular interactions, and baseline conditions, binocular interactions, and baseline conditions. J Neurosci 8(5):1500–1530
Tootell RBH, Switkes E, Silverman MS, Hamilton SL (1988) Functional anatomy of macaque striate cortex. II. Retinotopic organization. J Neurosci 8(5):1531–1568
Turing AM (1952) The chemical basis of morphogenesis. Phil Trans Roy Soc Lond B237:37–72
von der Malsburg Christof, Willshaw DJ (1977) How to label nerve cells so that they can interconnect in an ordered fashion. Proc Natl Acad Sci 74(11):5176–5178
Wicklein M, Strausfeld NJ (2000) Organization and significance of neurons that detect change of visual depth in the hawk moth manduca sexta. J Comp Neurol 424(2):356–376
Wiesel TN, Hubel DH (1974) Ordered arrangement of orientation columns in monkeys lacking visual experience. J Comp Neurol 158(3):307–318
Willshaw DJ, von der Malsburg C (1979) A marker induction mechanism for the establishment of ordered neural mappings: its application to the retinotectal problem. Philos Trans R Soc Lond Ser B 287:203–243
Wimbauer S, Gerstner W, van Hemmen JL (1998) Analysis of a correlation-based model for the development of orientation-selective receptive fields in the visual cortex. Netw Comput Neural Syst 9(4):449–466
Wimbauer S, Wenisch OG, Miller KD, van Hemmen JL (1997) Development of spatiotemporal receptive fields of simple cells: I. Model formulation. Biol Cybern 77:454–462
Wimbauer S, Wenisch OG, van Hemmen JL, Miller KD (1997) Development of spatiotemporal receptive fields of simple cells: II. Simulation and analysis. Biol Cybern 77:463–477
Wolf F, Geisel T (1998) Spontaneous pinwheel annihilation during visual development. Nature 395:73–78
Wolf F (2005) Symmetry, multistability, and long-range interactions in brain development. Phys Rev Lett 95(20):208701

Yao X, Jin L, Hu H (2007) Pinwheel patterns give rise to the direction selectivity of complex cells in the primary visual cortex. Brain Res 1170:140–146

Yuille AL, Kolodny JA, Lee CW (1996) Dimension reduction, generalized deformable models and the development of ocularity and orientation. Neural Netw 9(2):309–319